



Calhoun: The NPS Institutional Archive
DSpace Repository

Theses and Dissertations

1. Thesis and Dissertation Collection, all items

2012-06

Viability of Cross-Flow Fan for Vertical Take-Off and Landing Aircraft

Delagrange, Christopher T.

Monterey, California. Naval Postgraduate School

<http://hdl.handle.net/10945/7330>

Downloaded from NPS Archive: Calhoun



Calhoun is a project of the Dudley Knox Library at NPS, furthering the precepts and goals of open government and government transparency. All information contained herein has been approved for release by the NPS Public Affairs Officer.

Dudley Knox Library / Naval Postgraduate School
411 Dyer Road / 1 University Circle
Monterey, California USA 93943

<http://www.nps.edu/library>



**NAVAL
POSTGRADUATE
SCHOOL**

MONTEREY, CALIFORNIA

THESIS

**VIABILITY OF CROSS-FLOW FAN FOR VERTICAL
TAKE-OFF AND LANDING AIRCRAFT**

by

Christopher T. Delagrange

June 2012

Thesis Advisor:
Second Reader:

Garth V. Hobson
Anthony J. Gannon

Approved for public release; distribution is unlimited

THIS PAGE INTENTIONALLY LEFT BLANK

REPORT DOCUMENTATION PAGE			<i>Form Approved OMB No. 0704-0188</i>	
Public reporting burden for this collection of information is estimated to average 1 hour per response, including the time for reviewing instruction, searching existing data sources, gathering and maintaining the data needed, and completing and reviewing the collection of information. Send comments regarding this burden estimate or any other aspect of this collection of information, including suggestions for reducing this burden, to Washington headquarters Services, Directorate for Information Operations and Reports, 1215 Jefferson Davis Highway, Suite 1204, Arlington, VA 22202-4302, and to the Office of Management and Budget, Paperwork Reduction Project (0704-0188) Washington DC 20503.				
1. AGENCY USE ONLY (Leave blank)		2. REPORT DATE June 2012	3. REPORT TYPE AND DATES COVERED Master's Thesis	
4. TITLE AND SUBTITLE Viability of Cross-Flow Fan for Vertical Take-Off and Landing Aircraft			5. FUNDING NUMBERS TDSI/11-007/1A - NPS	
6. AUTHOR(S) Christopher T. Delagrange				
7. PERFORMING ORGANIZATION NAME(S) AND ADDRESS(ES) Naval Postgraduate School Monterey, CA 93943-5000			8. PERFORMING ORGANIZATION REPORT NUMBER	
9. SPONSORING /MONITORING AGENCY NAME(S) AND ADDRESS(ES) TDSI – National University of Singapore 21 Lower Kent Ridge Road Singapore, 119077			10. SPONSORING/MONITORING AGENCY REPORT NUMBER	
11. SUPPLEMENTARY NOTES The views expressed in this thesis are those of the author and do not reflect the official policy or position of the Department of Defense or the U.S. Government. IRB Protocol number _____N/A_____.				
12a. DISTRIBUTION / AVAILABILITY STATEMENT Approved for public release; distribution is unlimited			12b. DISTRIBUTION CODE	
13. ABSTRACT (maximum 200 words) The present study is focused on determining a housing design that, when paired with an off-the-shelf cross-flow fan rotor, will generate a trust-to-weight ratio significant enough to allow for vertical take-off. The commercial computational fluid dynamics software, ANSYS CFX, was used to perform a computational analysis of various housing designs until a suitable design was identified to construct for experimentation. Following the analytical phase, the conceptual housing was fabricated and paired with an appropriate rotor to validate the predicted performance. The experimental model was operated at speeds from 4,000 to 8,000 rpm and the actual and projected thrust calculations were found to agree with a maximum difference of less than 7%.				
14. SUBJECT TERMS Vertical take-off, VTOL, cross-flow fan, CFF			15. NUMBER OF PAGES 77	
			16. PRICE CODE	
17. SECURITY CLASSIFICATION OF REPORT Unclassified	18. SECURITY CLASSIFICATION OF THIS PAGE Unclassified	19. SECURITY CLASSIFICATION OF ABSTRACT Unclassified	20. LIMITATION OF ABSTRACT UU	

THIS PAGE INTENTIONALLY LEFT BLANK

Approved for public release; distribution is unlimited

**VIABILITY OF CROSS-FLOW FAN FOR VERTICAL TAKE-OFF AND
LANDING AIRCRAFT**

Christopher T. Delagrange
Lieutenant, United States Navy
B.S., University of Arizona, 2005

Submitted in partial fulfillment of the
requirements for the degree of

MASTER OF SCIENCE IN MECHANICAL ENGINEERING

from the

**NAVAL POSTGRADUATE SCHOOL
June 2012**

Author: Christopher T. Delagrange

Approved by: Garth V. Hobson
Thesis Advisor

Anthony J. Gannon
Second Reader

Knox T. Milsaps
Chair, Department of Mechanical and Aerospace Engineering

THIS PAGE INTENTIONALLY LEFT BLANK

ABSTRACT

The present study is focused on determining a housing design that, when paired with an off-the-shelf cross-flow fan rotor, will generate a thrust-to-weight ratio significant enough to allow for vertical take-off. The commercial computational fluid dynamics software, ANSYS CFX, was used to perform a computational analysis of various housing designs until a suitable design was identified to construct for experimentation. Following the analytical phase, the conceptual housing was fabricated and paired with an appropriate rotor to validate the predicted performance. The experimental model was operated at speeds from 4,000 to 8,000 rpm and the actual and projected thrust calculations were found to agree with a maximum difference of less than 7%.

THIS PAGE INTENTIONALLY LEFT BLANK

TABLE OF CONTENTS

I.	INTRODUCTION.....	1
A.	OVERVIEW	1
B.	BACKGROUND	1
C.	OBJECTIVE	4
II.	DESCRIPTION OF THE ANALYTICAL MODEL.....	5
A.	OVERVIEW	5
B.	SOLID MODELING	5
C.	MESH GENERATION AND BOUNDARY CONDITIONS.....	7
1.	Mesh Generation.....	7
2.	Established Boundary Conditions and Analysis	9
D.	SIMULATION PLAN	11
III.	EXPERIMENTAL SETUP	13
A.	SOLIDWORKS DESIGN AND FABRICATION	13
B.	BENCHTEST SETUP	15
1.	Test Rig	15
2.	Cross-Flow Fan Control.....	17
3.	Data Acquisition and Instrumentation	17
C.	REDUCTION OF TEST DATA	21
IV.	RESULTS AND DISCUSSION	23
A.	CONVERGENCE OF ANALYTICAL RESULTS	23
B.	FLOW VISUALIZATION.....	24
C.	ANALYTICAL VERSUS EXPERIMENTAL RESULTS.....	26
1.	Thrust.....	26
2.	Velocity Profiles	28
3.	Power.....	33
V.	CONCLUSION AND RECOMMENDATIONS.....	35
A.	THRUST TO WEIGHT RATIO	35
B.	HOUSING AND ROTOR DESIGN	35
C.	RECOMMENDATIONS.....	36
	APPENDIX A. ASSEMBLY DESIGN PROCESS	37
A.	ROTOR SELECTION.....	37
B.	HOUSING DESIGN	39
	APPENDIX B. ANSYS CFX SETTINGS AT 8,000 RPM	41
	APPENDIX C. CFF COMPONENT DRAWINGS	47
	APPENDIX D. VELOCITY DATA FOR 8,000 RPM OUTLET	55
	LIST OF REFERENCES.....	57
	INITIAL DISTRIBUTION LIST	59

THIS PAGE INTENTIONALLY LEFT BLANK

LIST OF FIGURES

Figure 1.	Commercial cross-flow fan (CFF) with 12-inch span	1
Figure 2.	Typical fan housing setup. From [1].....	2
Figure 3.	CFD simulation of the Propulsive Wing at a high angle of attack. From [7]....	3
Figure 4.	SOLIDWORKS model of 16-blade rotor	6
Figure 5.	SOLIDWORKS model of CFF housing	6
Figure 6.	Fine mesh generated in the CFF assembly	8
Figure 7.	Detail of fine mesh showing single element thickness	8
Figure 8.	Locations of CFF boundaries.....	9
Figure 9.	Inlet (a) and outlet (b) views of CFF concept.....	13
Figure 10.	Exploded view of CFF concept.....	14
Figure 11.	Basic test rig setup with Bosch 14 amp router.....	15
Figure 12.	Test rig with side walls attached and outlet flow normal to the ground	16
Figure 13.	Final operational model	16
Figure 14.	Rheostat for controlling voltage to the Bosch router	17
Figure 15.	Ammeter used to measure router supply current	18
Figure 16.	Tri-beam balance below CFF outlet	18
Figure 17.	Course pressure sensing array.....	19
Figure 18.	Pressure rake probe	20
Figure 19.	Setup for stagnation pressure data collection.....	21
Figure 20.	Convergence of mass flow rate at 8,000 rpm	23
Figure 21.	Convergence of rotor torque at 8,000 rpm.....	24
Figure 22.	Air velocity through CFF operating at 8,000 rpm	25
Figure 23.	Air velocity streamlines in CFF operating at 8,000 rpm	26
Figure 24.	Experimental and analytical thrust calculations	27
Figure 25.	Comparison of experimental to analytical outlet velocity	30
Figure 26.	Outlet velocity profile using grid probe, 8,000 rpm	30
Figure 27.	Outlet velocity profile using rake probe, 8,000 rpm.....	31
Figure 28.	Comparison of experimental and analytical velocity profiles from experimental fine mesh data	32
Figure 29.	Experimental and analytical power calculations.....	33
Figure 30.	DFA32 series DC CFF rotor.....	37
Figure 31.	ANSYS STRUCTURAL safety factor investigation of rotor at 10,000 rpm ..	38
Figure 32.	Velocity streamlines through initial housing design.....	39
Figure 33.	Velocity streamlines through the second proposed housing.....	40

THIS PAGE INTENTIONALLY LEFT BLANK

LIST OF TABLES

Table 1.	CFF assembly mesh statistics	7
Table 2.	CFF Assembly components	14
Table 3.	ANSYS CFX data for analytical thrust calculation	27
Table 4.	Thrust measurements from CFF test rig	28
Table 5.	Velocity measurements from grid probe, 4,000 rpm (m/s).....	28
Table 6.	Velocity measurements from grid probe, 6,000 rpm (m/s).....	29
Table 7.	Velocity measurements from grid probe, 8,000 rpm (m/s).....	29

THIS PAGE INTENTIONALLY LEFT BLANK

LIST OF ACRONYMS AND ABBREVIATIONS

2D	Two-Dimensional
A	Area (m ²)
a _i	Elemental area
CFX Pre	Part of the ANSYS-CFX package for application of boundary and initial conditions as well as solver settings
CFD	Computational fluid dynamics
CFF	Cross-flow fan
δ	Nondimensional total pressure correction term (P_T/P_{Tstd})
DC	Direct current
DSA	Digital sensing array
ε	Viscous dissipation
g	gram
h	Enthalpy
HVAC	Heating ventilation and cooling
I	Current
ID	Inside diameter
k	Turbulent kinetic energy
K	Degree Kelvin
kg	Kilogram
λ	Thermal conductivity (W/mK)
LiPo	Lithium polymer
LTV	Ling-Temco-Vought
μ	Dynamic viscosity

μ_t	Turbulent viscosity
m	meter
mm	millimeter
N	Newton
OD	Outside diameter
p	Pressure
p_o	Total Pressure
Pa	Pascal
ρ	Density
RC	Remote control
rpm	Revolutions per minute
s	second
S_E	Energy source equation
S_M	Momentum source equation
SOLIDWORKS	Three-dimensional drafting and solid modeling software package
T	Temperature
T_t	Total temperature
TPL	Turbopropulsion laboratory
U	Velocity
V	Voltage
VSD	Vought Systems Division
VTOL	Vertical take-off and landing
WORKBENCH	ANSYS simulation package which ties external CAD software together with the ANSYS suite finite element software

ACKNOWLEDGMENTS

I would like to express my gratitude and appreciation to the following people:

Professor Garth Hobson, for his encouragement, never-ending optimism and genuine excitement about the thesis research I conducted.

Professor Anthony Gannon, for allowing me to tap into his seemingly endless knowledge of CFD analysis, and assisting me with any questions I could devise for him.

John Gibson, for his assistance and patience in helping me with every aspect of my CFF model fabrication.

Professor Tim Sands, for making my first NPS class a wonderful experience and helping me to jump-start my thesis research.

Finally, with a tremendous amount of love, I thank my wife, Mellisa, and children, Sebastian, Josephine and Natallie, for their support, encouragement and understanding.

THIS PAGE INTENTIONALLY LEFT BLANK

I. INTRODUCTION

A. OVERVIEW

Vertical take-off and landing (VTOL) aircraft perform a number of different functions in the world today, so there has been a recent resurgence in interest to find an alternate method of propulsion that is simpler than today's VTOL fixed-wing aircraft and safer than rotary-wing aircraft. A propulsion system designed around a cross-flow fan (CFF) is an ideal candidate for the VTOL vehicle of the future. The ability to embed the fan's rotor in the wing of an aircraft would allow for a large span for thrust generation, and thrust produced by a CFF can be easily vectored using control surfaces, which eliminates the design challenge of rotating the fan rotor and prime mover. Additionally, having the rotor imbedded in the aircraft's wing eliminates the safety concern of a rotary wing's exposed blades.

B. BACKGROUND

The CFF was initially patented over a century ago and its low profile, large span design has made it ideal for a number of applications both large and small. Today, CFFs can be found in heating ventilation and cooling (HVAC) systems, air curtains designed to maintain a boundary between two atmospheres, and within computer servers to circulate cooling air. Figure 1 is an example of a commercial CFF used to circulate air in a computer tower.



Figure 1. Commercial cross-flow fan (CFF) with 12-inch span

Vought Systems Division (VSD) of the Ling-Temco-Vought (LTV) Aerospace Corporation first explored the CFF as a means of propulsion when they were awarded a Navy contract, in 1975, to explore new thrust augmenting concepts for the development of subsonic transport aircraft [1]. In the VSD study, many different rotor designs and housing configurations were analyzed and tested, which resulted in 46 prospective configurations of 12-inch-diameter fans. Figure 2 shows the typical CFF setup used for testing by VSD. While VSD did conclude that a CFF was capable of producing the thrust required for aircraft propulsion, the company did not continue the research or build a prototype for flight.

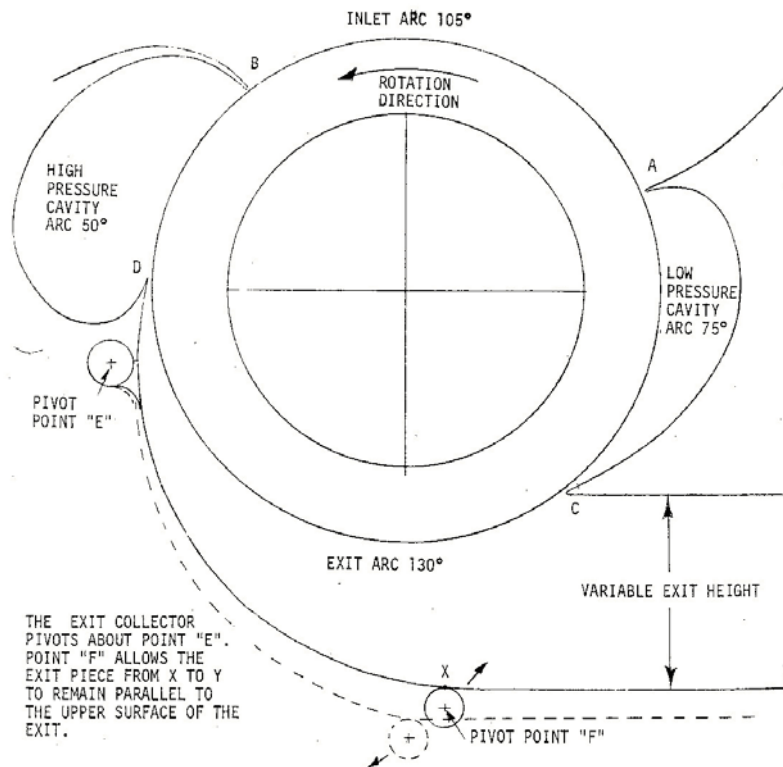


Figure 2. Typical fan housing setup. From [1]

The next two decades saw little advancement of the initial research conducted by VSD. In 2000, researchers at the Naval Postgraduate School's Turbo-propulsion Laboratory (TPL) sparked resurgence in the interest of CFF propulsion when Gossett [2] proposed using a CFF to augment the vertical thrust of a single seat VTOL aircraft. Gossett's design included VSD's #6 CFF assembly imbedded in the nose of the aircraft to

provide additional vertical thrust. Since then, a number of other researchers at the TPL have continued to study the CFF as a means of aircraft propulsion. In 2003, Cheng [3] performed an experimental and numerical analysis of a 12-inch diameter, 1.5-inch span CFF. The aim of Cheng's research was to validate VSD's research and develop a computational model of the CFF that could be further used for design modifications and improvements. Following Cheng's validation research, Schreiber and Ulvin [4], [5] continued researching the performance of CFF rotors by modeling rotors of a smaller, 6-inch diameter, over a range of spans from 1.5 inches to 6 inches. Most recently, Antoniadis [6] has investigated altering the blade design and the number of blades on a CFF rotor to optimize its performance. Antoniadis found that the previously tested 30-blade designs were not optimum for thrust production. He used CFD analysis, validated through experimentation, to prove that a 22-blade rotor was both more efficient and generated a higher thrust-to-power ratio than the 30-blade rotor for all operating speeds.

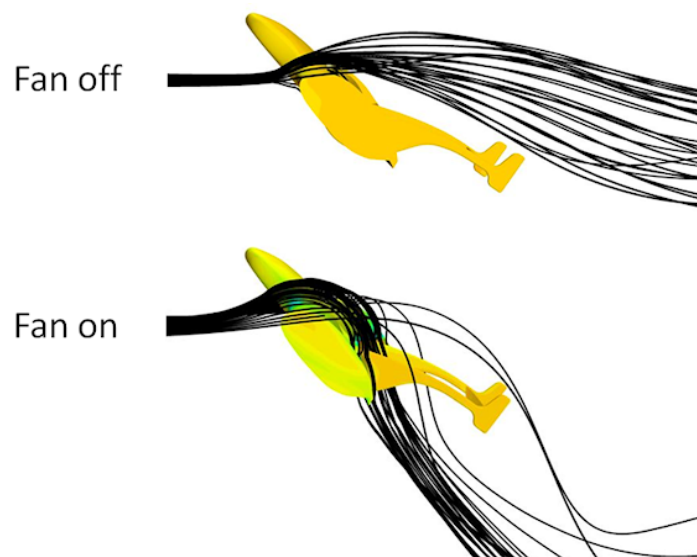


Figure 3. CFD simulation of the Propulsive Wing at a high angle of attack. From [7]

In 2006, Propulsive Wing patented a new aerodynamic platform that integrates an embedded, distributed cross-flow fan propulsion system within a thick wing [7]. While the current Propulsive Wing models do not have the capability for VTOL, the company has developed an aircraft whose sole means of propulsion is via a CFF. Additionally, as can be seen in Figure 3 and in videos on their website, the Propulsive Wing is capable of

near vertical hovering when the plane is oriented at a steep angle of attack, with the CFF operating. The Propulsive Wing demonstration gives much gives much optimism to the future of CFF powered VTOL aircraft.

C. OBJECTIVE

The aim of this thesis is to analytically model a CFF housing that will result in a thrust-to-weight ratio of greater than one, and therefore produce a CFF propulsion system that is capable of VTOL. After a suitable model has been developed, then an experimental model will be fabricated and tested to validate ANSYS CFX as a reliable method for CFF design.

II. DESCRIPTION OF THE ANALYTICAL MODEL

A. OVERVIEW

A commercial computational fluid dynamics (CFD) software package, ANSYS-CFX, was used to model the flow through a two-dimensional (2D) CFF assembly. Designing a CFF housing that would run effectively over a large range of operating speeds was a highly iterative process and the use of CFX allowed for relatively quick flow analysis of each proposed design. During the housing modeling and selection portion of the analysis, a course mesh with less than 100,000 nodes was used to allow for rapid computation and a relative estimation of the CFF performance against other housing designs. After identifying a housing that performed well with the coarse settings, a mesh refinement was then performed to confirm the results and attain a more accurate prediction of the CFF flow characteristics for eventual comparison with experimental data. The design process for the CFF assembly is described in detail in Appendix A.

B. SOLID MODELING

The commercial 3D computer-assisted drafting (CAD) software, SOLIDWORKS, was used for all of the modeling of the proposed CFF designs. Figure 4 shows the SOLIDWORKS rotor model which is based on a 78 mm diameter, 210 mm span, carbon fiber rotor fabricated by DragonPlate Carbon Fiber Composites. This rotor was selected for use based on its light weight and maximum speed rating of 8,000 rpm. The outer diameter of the SOLIDWORKS rotor domain is 80 mm to allow for a 1 mm clearance between the rotor domain and the housing domain. This clearance was designed so that when paired with the housing domain, a total clearance of 2 mm would be achieved between the walls of the housing and the blade tips on the rotor. The thickness of the rotor domain and housing domain is 0.2 mm to ensure that the diameter-to-depth ratio is very high, so that ANSYS-CFX will only analyze the 2D flow characteristics.

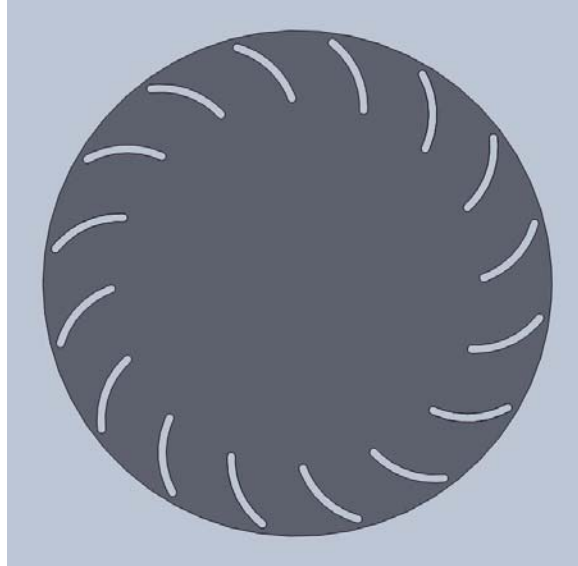


Figure 4. SOLIDWORKS model of 16-blade rotor



Figure 5. SOLIDWORKS model of CFF housing

Figure 5 is an image of the SOLIDWORKS model of the housing domain used in the CFD analysis. The housing domain is similar to the CFF model in Figure 2, and is based on a housing design initially proposed by VSD [1]. The extruded cut through the center has a diameter of 80 mm so that rotor domain can be paired with the housing at this interface. This design eliminates both of the high pressure and low pressure cavities proposed by VSD. Cheng's [3] research showed that there was not a significant change

in the performance of a 30-blade, 12-inch rotor when it was operated with and without the cavities. To provide a housing that can be manufactured more easily, these cavities were not included in the design.

C. MESH GENERATION AND BOUNDARY CONDITIONS

1. Mesh Generation

The initial mesh for the CFD model contained 98,594 nodes which made up 47,444 elements. This coarse mesh was acceptable for a gross estimation of air flow through the CFF during the initial design phase, but after an acceptable housing design was identified, the mesh needed to be refined for a more accurate estimation of the assembly's performance. Two mesh refinements were performed on the initial coarse mesh with a goal of generating greater than 500,000 nodes while still maintaining a mesh thickness of one element. Table 1 lists the mesh statistics generated during each phase of refinement. This refinement was performed to have a sufficiently high mesh resolution throughout the domain to accurately predict the turbulent environment in the unsteady flow field. While the method of mesh generation is significantly different than the mesh generated by Yu [8] during his analysis, the resulting mesh is comparable and as he proved through comparisons, results in an accurate representation of experimental data when used in conjunction with the k-epsilon turbulence model.

Table 1. CFF assembly mesh statistics

	Nodes	Elements
Mesh #1	98,594	47,444
Mesh #2	337,066	162,735
Mesh #3	501,890	243,870

Figure 6 shows the final mesh obtained for CFD analysis. This mesh consists of 501,890 nodes that are connected to form 243,870 elements. Figure 7 details a rotated

highlight of a section at the rotor domain and housing domain interface. From this picture, it can be seen that the required single-element thickness has been maintained on both of the CFF domains.

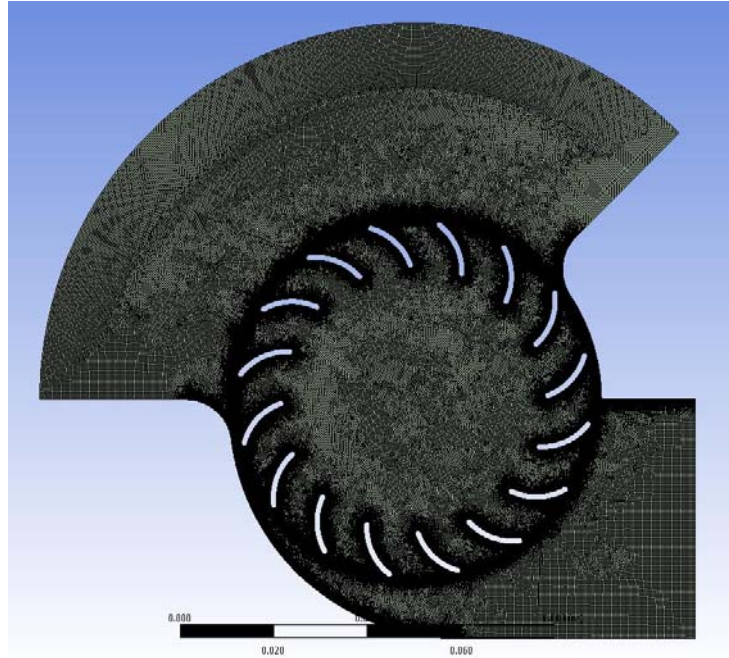


Figure 6. Fine mesh generated in the CFF assembly

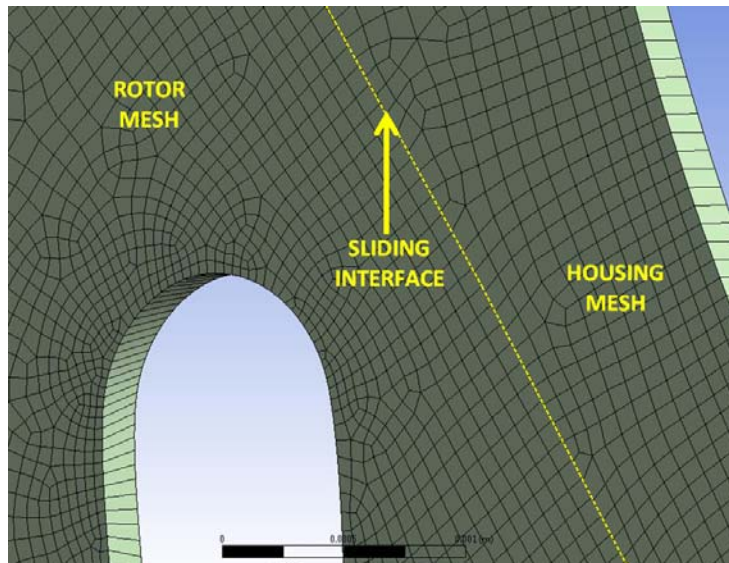


Figure 7. Detail of fine mesh showing single element thickness

2. Established Boundary Conditions and Analysis

ANSYS-WORKBENCH was the core program used to coordinate all steps of the CFD analysis. After creating and meshing the two SOLIDWORKS models, they were imported into CFX Pre as two components connected at the rotor-housing interface. This interface was formed so that during analysis the housing domain would remain fixed in space, but the rotor domain was free to move about its axis at a rotational velocity specified by the user. Figure 8 shows the user defined regions of the CFF assembly that were established during the meshing phase. Each of these named areas was imported into CFX Pre so that appropriate boundary conditions could be defined. All black walls in the figure were undefined, so they became parts of the rotor and housing default domains and were therefore treated as no-slip walls during the analysis.

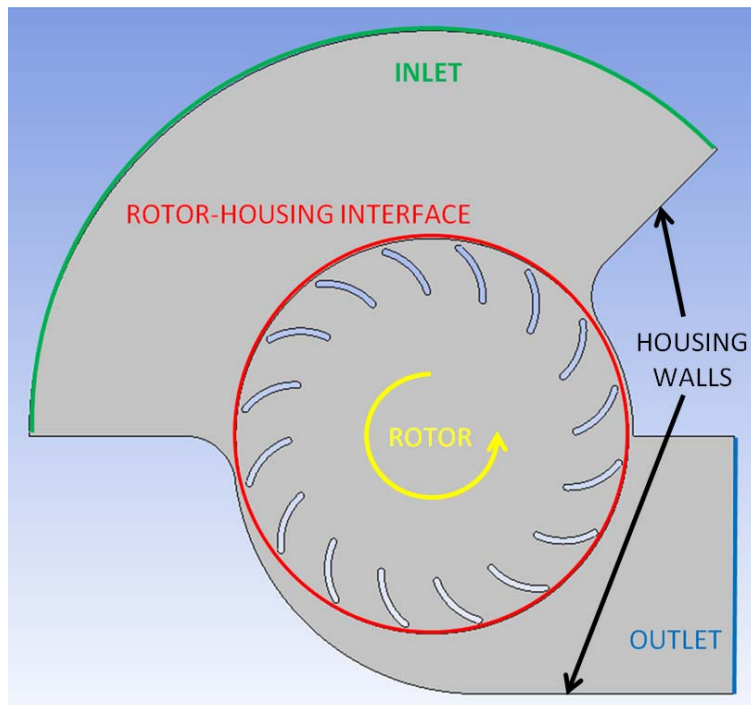


Figure 8. Locations of CFF boundaries

Each CFD analysis was conducted as a transient analysis with the total time and time steps adjusted to allow for five revolutions of the rotor at one degree per time step. This resulted in a final RMS Courant number of about 7. The housing and rotor domain

shared almost the same initial conditions, running with air as an ideal gas at a relative pressure of 1 atmosphere and a temperature of 288.15 K, and a turbulence intensity factor of 5%. The total energy model and k-epsilon turbulence model were selected to account for energy input into the rotor and turbulence in the air flow. The only difference in the domains' setups was that the housing domain was modeled as a stationary object, and the rotor domain was set to rotate about its axis at a defined angular velocity.

The housing inlet was modeled as an opening with a 0 Pa stagnation pressure, due to the uncertainty of flow direction as the rotor begins to spin. Similarly, the outlet was also modeled as an opening, but with a 0 Pa average static pressure at its boundary. Each face of the housing and rotor were modeled as symmetry planes so that the resultant analysis would be a true 2D representation of an infinitely long CFF. Finally, a domain interface was established at the rotor-housing boundary to allow for communication between the two regions during analysis. With the appropriate boundary conditions established, CFX solver uses the following equations during the CFD analysis:

Continuity equation:

$$\frac{\partial \rho}{\partial t} + \nabla \cdot (\rho U) = 0 \quad (1)$$

Momentum equation:

$$\frac{\partial \rho U}{\partial t} + \nabla \cdot (\rho U \otimes U) = \nabla \cdot \left(-p \delta + \mu \left(\nabla U + (\nabla U)^T \right) \right) \quad (2)$$

Energy equation:

$$\frac{\partial \rho h_{tot}}{\partial t} - \frac{\partial \rho}{\partial t} + \nabla \cdot (\rho U h_{tot}) = \nabla \cdot (\mu \nabla T) + \nabla \cdot \left(\mu \nabla U + \nabla U^T - \frac{2}{3} \nabla \cdot U \delta U \right) \quad (3)$$

$$h_{tot}(p, T) = h_{stat}(p, T) + \frac{1}{2} U^2 \quad (4)$$

Turbulent eddy viscosity:

$$\mu_t = C_\mu \rho \frac{\kappa^2}{\varepsilon} \quad (5)$$

Turbulent kinetic energy:

$$\frac{\partial(\rho k)}{\partial t} + \nabla \cdot (\rho U k) = \nabla \cdot \left[\left(\mu + \frac{\mu_t}{\sigma_\kappa} \right) \nabla k \right] + P_k - \rho \varepsilon \quad (6)$$

Turbulent eddy dissipation:

$$\frac{\partial(\rho \varepsilon)}{\partial t} + \nabla \cdot (\rho U \varepsilon) = \nabla \cdot \left[\left(\mu + \frac{\mu_t}{\sigma_\varepsilon} \right) \nabla \varepsilon \right] + \frac{\varepsilon}{\kappa} (C_{\varepsilon 1} P_\kappa - C_{\varepsilon 2} \rho \varepsilon) \quad (7)$$

The equation of state:

$$\rho(p, T) = \frac{p}{R_0 T} \quad (8)$$

D. SIMULATION PLAN

The CFD simulation plan was developed to predict the performance of the CFF design over a range of speeds from 4,000 to 8,000 rpm. All of the simulations began with the same initial conditions at the inlet and outlet of 0 Pa stagnation pressure and static pressure, respectively. Additionally, the initial air velocities normal to each of these boundaries was set at 0 m/s to represent the initial conditions of a stationary VTOL aircraft prior to take off. Each prospective CFF design was initially simulated to run for five revolutions at 4,000 rpm. If the design performed well then the simulation was advanced to 6,000 rpm and then finally 8,000 rpm. Good model performance was defined as a geometry that generated thrust, showed no indications of stall for a majority of the blades, with convergence of rotor torque to a constant value, and had the difference in inlet and outlet mass flow rate converge to zero. The ANSYS CFX settings are listed in Appendix B.

THIS PAGE INTENTIONALLY LEFT BLANK

III. EXPERIMENTAL SETUP

A. SOLIDWORKS DESIGN AND FABRICATION

Successful completion of the analytical phase of the CFF design led to modeling a complete version of the prospective housing in SOLIDWORKS so that the entire assembly could be fabricated and experimentation could be performed to validate the results from CFD analysis. The shape of the cross-section of the proposed design was defined by the profile of the model used during computational analysis. The wall profiles were given a small thickness and extruded out to match the length of the rotor so that the housing could be formed. Each of the endplates was designed as 2 mm thick aluminum plates to add rigidity to the relatively thin housing walls. The bearing housing was also designed to be fabricated from aluminum to minimize weight of the assembly. A 6 mm stainless steel shaft was selected to connect the rotor to the bearing, and finally all mounting hardware and brackets were included to complete to full CFF assembly. Figure 9 shows the entire assembled model and the exploded view in Figure 10 gives full details of the component locations for construction. Additional details of the designed components can be found in Appendix C.

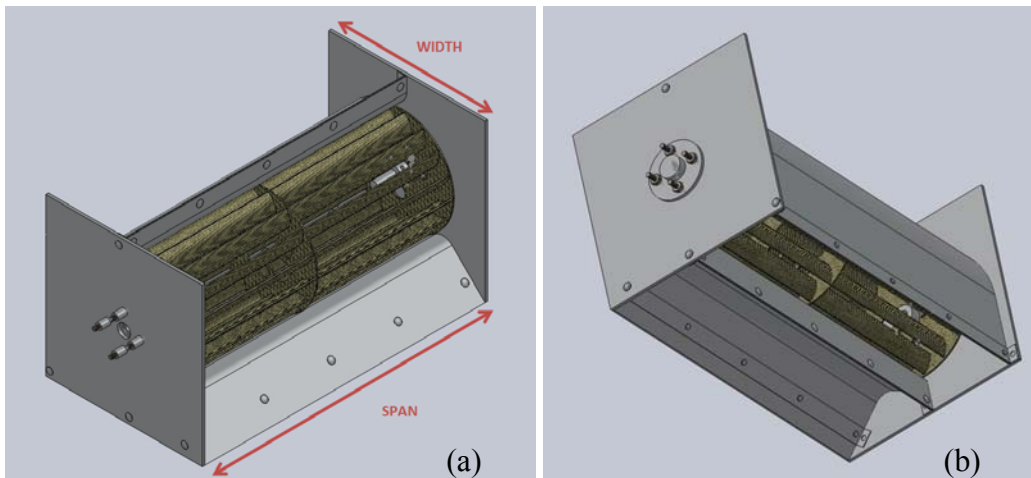


Figure 9. Inlet (a) and outlet (b) views of CFF concept

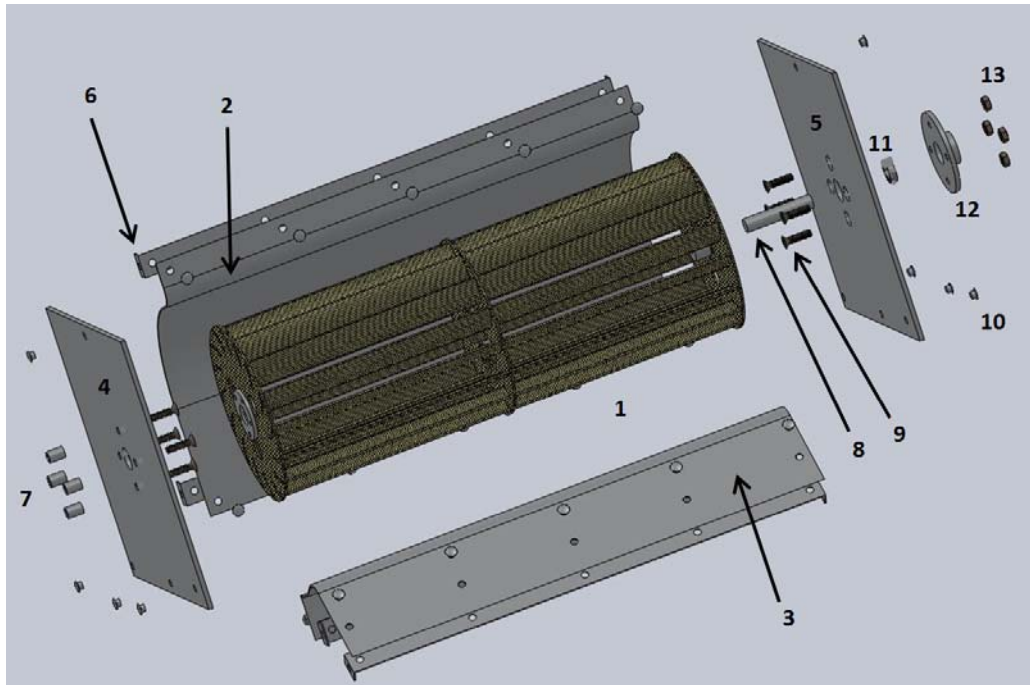


Figure 10. Exploded view of CFF concept

Table 2. CFF Assembly components

1	16-Blade Carbon Fiber Rotor
2	Aluminum Housing Wall #1
3	Aluminum Housing Wall #2
4	Aluminum Motor-End Support Plate
5	Aluminum Bearing-End Support Plate
6	Housing Wall Support Brackets (4)
7	Motor Stand-Offs
8	6 mm Stainless Steel Shaft
9	3M Countersunk Screws (8)
10	1/8" Aluminum Rivets (28)
11	Stainless Steel Ball Bearing, 10 mm OD, 6 mm ID
12	Bearing Housing
13	Stainless Steel Nuts (4) [optional, based on threading the bearing housing]

B. BENCHTEST SETUP

1. Test Rig

The initial setup for testing the CFF housing can be seen in Figure 11, and was comprised of two heavy endplates with the rotor mounted between them. In the figure, the left plate has a bearing housing attached which contains a bearing to support that end of the rotor. A 14 amp Bosch router is rigidly attached to the right bracket and holds a shaft connected to the rotor. This bulky setup was used for the initial testing because the heavy aluminum brackets were needed to support the weight of the router and the open design allowed for temporary attachment of virtually any conceived housing design.

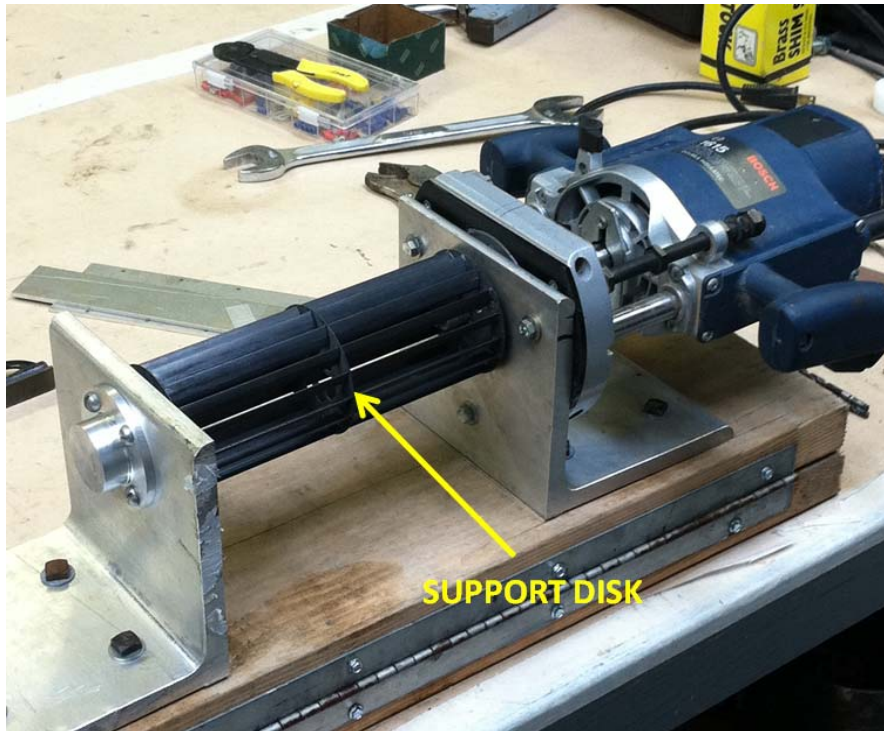


Figure 11. Basic test rig setup with Bosch 14 amp router

Figure 12 shows the test rig, with attached housing walls, mounted to a work table and oriented in the testing position. For testing the outlet of the CFF was oriented such that the air flow leaving the housing was perpendicular to the ground. This orientation was selected because the rotor was clearly visible for the use of a strobe tachometer and thrust measurements could be easily taken with a simple triple-beam balance.



Figure 12. Test rig with side walls attached and outlet flow normal to the ground

Following the successful testing of the proposed housing design using the test rig shown in Figure 12, a light weight operational model was built to verify that the thrust produced by the CFF was sufficient to provide the desired vertical take-off capability. The parts for this model were fabricated from the SOLIDWORKS model specifications and the final assembly can be seen in Figure 13.



Figure 13. Final operational model

2. Cross-Flow Fan Control

Control of the CFF rotor speed was made possible by using a rheostat, shown in Figure 14, to control the voltage being supplied to the Bosch router. The rheostat was used to regulate the percentage of the 110 V supply voltage that was supplied to the router. A strobe tachometer was set at the desired rotor speed and the routers supply voltage was adjusted until the CFF rotor speed matched the speed set on the tachometer.



Figure 14. Rheostat for controlling voltage to the Bosch router

3. Data Acquisition and Instrumentation

The CFF power consumption was measured to determine the electrical power that would be required for operation at various rotor speeds, to compare to the mechanical power generated by the CFF for determination of efficiency, and to compare to the analytically determined power for validation of the computer model. The voltage supplied to the router was known based on the setting of the rheostat used for router speed control. A clip-on ammeter (Figure 15) was used to measure the current supplied to the router.



Figure 15. Ammeter used to measure router supply current

Two independent thrust measurements were calculated during the experimentation phase. Figure 16 shows the assembly setup for the first method of measuring the CFF thrust. A tri-beam balance was oriented under the CFF outlet such that the flow leaving the fan was perpendicular to the surface of the sample pan. The balance's pan was of sufficient size to ensure that the entire flow area at the outlet made contact with the balance. This setup allowed for a direct thrust measurement in grams by balancing the scale and reading the counter-balance weight required to zero the scale.

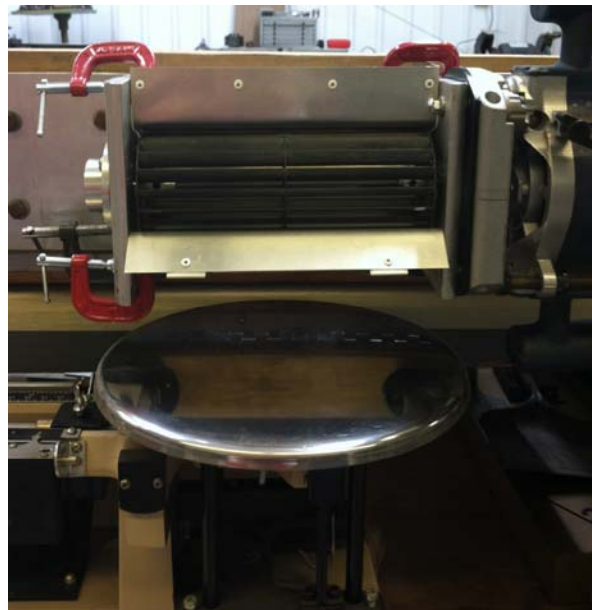


Figure 16. Tri-beam balance below CFF outlet

The second method used to determine the CFF's thrust was through the use of the average air velocity leaving the fan. Initially, a hand-held anemometer was used to find the outlet velocity, but the variations in measurement were erratic and the measurements were extremely sensitive to the probe's location. Outlet velocity was instead found by measuring the stagnation pressure at the outlet plane using an array of pressure ports. Figures 17 and 18 show the two different probe arrangements used. The probe array in Figure 17 was constructed to match the area of the flow through the fan's outlet. This probe was effective, but the variation in air velocity throughout the measured area was too extreme for the course array to accurately resolve. The rake probe in Figure 18 was assembled to more accurately resolve the true velocity profile. The rake probe used 16 pressure ports, 4 mm apart, and the probe was traversed at 5 mm increments across the outlet plane to generate a fine array of 688 measurement points.

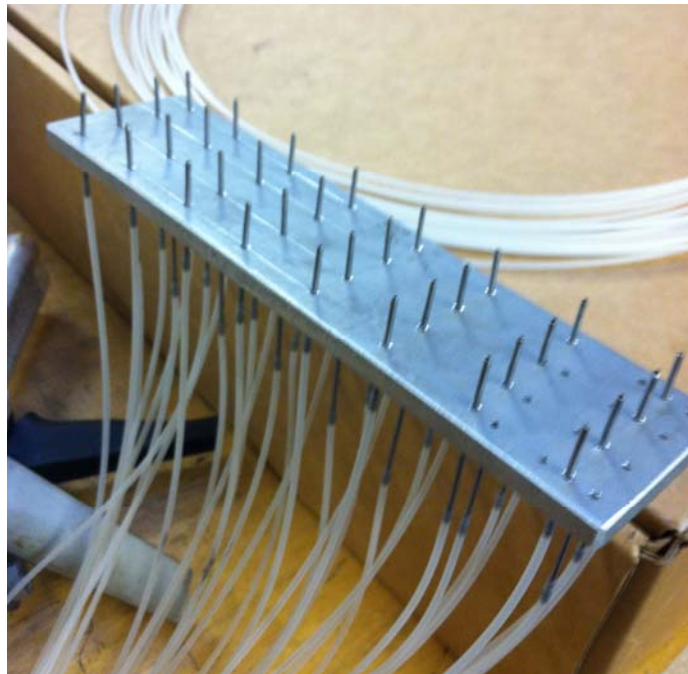


Figure 17. Course pressure sensing array

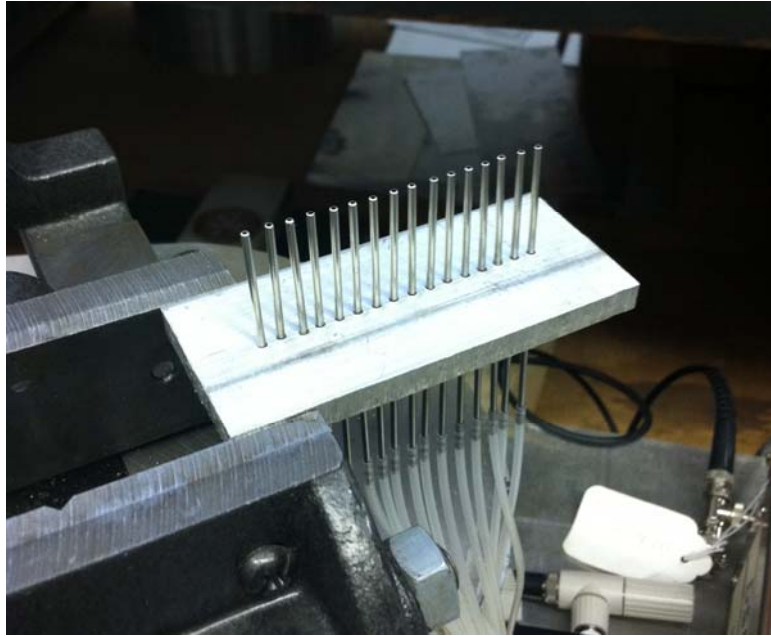


Figure 18. Pressure rake probe

Figure 19 shows the CFF assembly setup for measuring the outlet stagnation pressures with the course pressure port array. The air tubes from the pressure ports were connected to the sensing ports of a Scanivalve digital sensing array (DSA), to convert the mechanical pressures into analog electrical signals. The DSA then converted the analog signal to a digital signal which was then acquired by a computer via an Ethernet connection. A Windows-based data acquisition program, Agilent VEE, was used to collect the resulting stagnation pressure readings and write them to a .txt file for future manipulation using the MATLAB software package.



Figure 19. Setup for stagnation pressure data collection

C. REDUCTION OF TEST DATA

In order to get an understanding of the CFF experimental performance and compare the results to the analytical model the mass flow rate, thrust and power needed to be calculated from the total pressure, voltage and current measurements. Each of these calculations was performed for the CFF speeds investigated in the simulation plan.

To determine the mass flow rate through the CFF, the pressures measured using the rake probe had to first be used to find the velocity at each point on the outlet plane. Equation 9 was used to find the velocity at each point in the array using the difference in total and static pressure from the DSA.

$$V_i = \sqrt{2 \frac{(p_{o_i} - p_{s_i})}{\rho}} \quad (9)$$

Each of the local velocities calculated were then combined to find the average velocity of the air leaving the CFF. Equation 10 was used to perform this calculation, where a_i was the element area surrounding each of the pressure ports.

$$\bar{V} = \frac{\int V dA}{\int dA} = \frac{\sum a_i V_i}{A} \quad (10)$$

With the average velocity calculated, the mass flow rate through the CFF was then calculated using Equation 11.

$$\dot{m} = \int \rho V dA = \rho_{air} A \bar{V} \quad (11)$$

Next the thrust force was obtained from Equation 12, assuming that the inlet air velocity was zero.

$$F_{thrust} = \int \rho V^2 dA = \rho_{air} \sum V_i^2 a_i \quad (12)$$

The mechanical power could then be determined using;

$$P_{mech} = F_{thrust} V = \int \rho V^3 dA = \rho_{air} \sum V_i^3 a_i \quad (13)$$

Finally, the electrical power consumed during CFF operation was found for each of the fan's operating speeds, so that an appropriate motor and power supply could be selected for the final operational model. Equation 14 was used for these calculations, with V being the voltage read on the rheostat and I the current read on the clip-on ammeter.

$$P_{elec} = VI \quad (14)$$

IV. RESULTS AND DISCUSSION

A. CONVERGENCE OF ANALYTICAL RESULTS

In Yu's [8] study of an analytical model of a CFF, he found that the mass flow rate, total pressure ratio, total temperature ratio and efficiency all converged to their steady state values after five revolutions of the model. Figure 20 shows the convergence history for mass flow rate through the CFF. The inlet mass flow rate and outlet mass flow rate were verified to reach a steady-state value after five revolutions. Additionally, the difference in these mass flow rates was calculated to verify that conservation of mass is satisfied during this simulation. After five revolutions, the difference in inlet and outlet mass flow rates was $9.32\text{E-}7$ kg/s which was 0.27 percent of the total flow rate through the CFF.

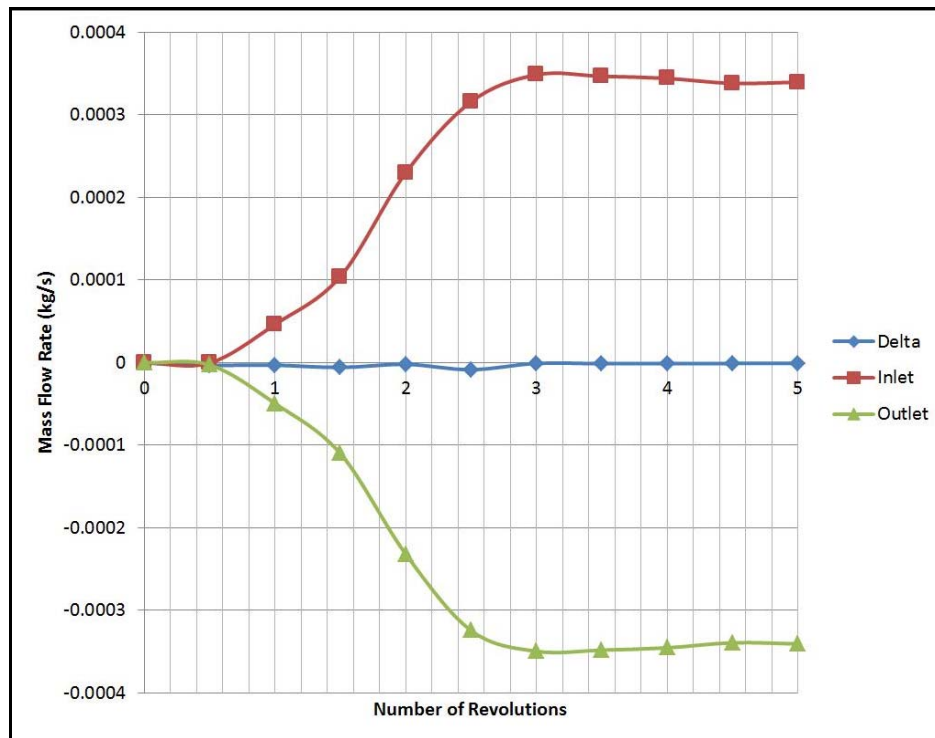


Figure 20. Convergence of mass flow rate at 8,000 rpm

In this simulation, the convergence of rotor torque was also analyzed over five complete revolutions. As seen in Figure 21, rotor torque also stabilized to a steady-state value of $7.29\text{E-}4$ N-m after the five revolutions were complete.

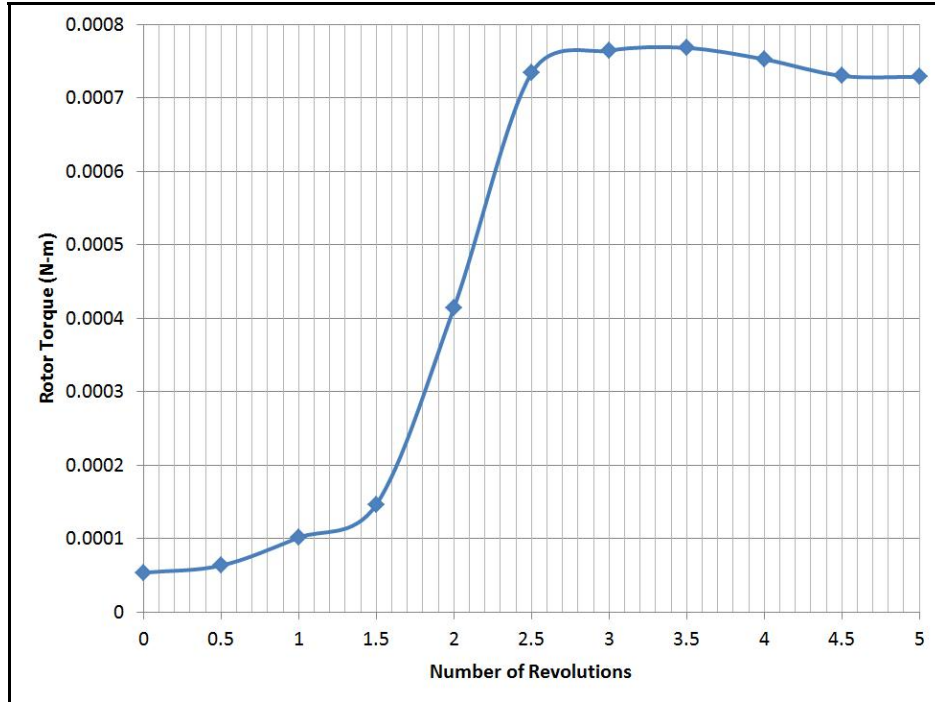


Figure 21. Convergence of rotor torque at 8,000 rpm

B. FLOW VISUALIZATION

Figure 22 shows the flow through the CFF during operation at 8,000 rpm. The formation of a vortex on the right side of the inner rotor can be observed. This vortex formation was expected and agrees with the observation in [8]. Unlike other models tested, which are described in further detail in Appendix A, this model displayed very little rotor-blade tip leakage in the region where the blades travel from the outlet back to the inlet. The observed tip leakage was prevented through the addition of the sharp corner between the housing wall and outlet duct. It was found that a fillet in this location allowed the vortex to entrain and guide flow from the outlet to the inlet.

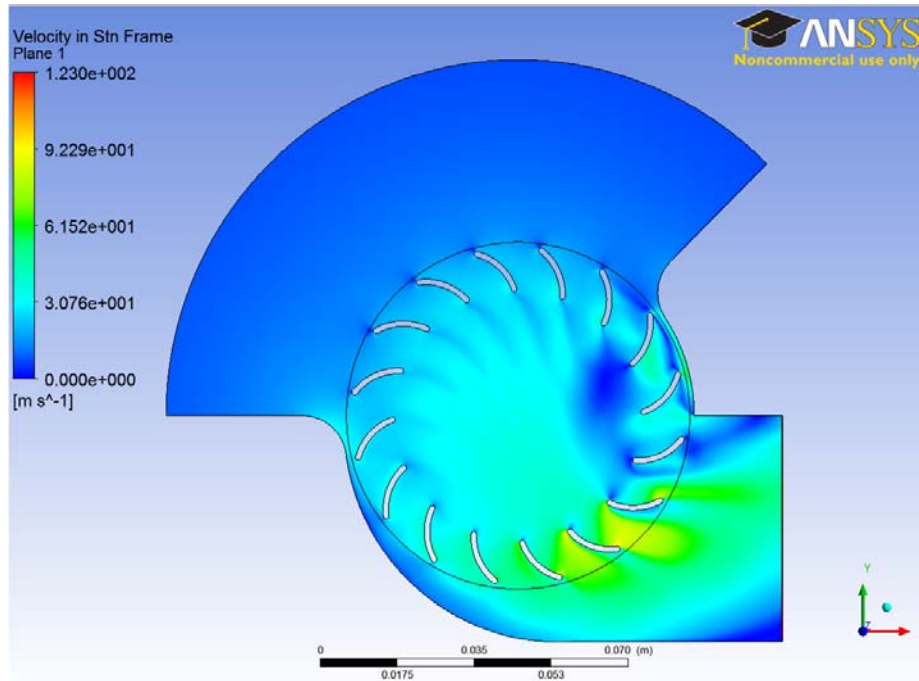


Figure 22. Air velocity through CFF operating at 8,000 rpm

Figure 23 shows the velocity streamlines that were developed in the model at 8,000 rpm. This figure illustrates that the CFF design does not have stalled rotor blades across the entire inlet area surface. The only stalled sections can be seen in the blade section that are traveling past the housing walls, where these blades would not be expected to be working on the fluid. The results of this design are similar to the results found by Antoniadis [6]. The flow fields observed in Figures 22 and 23 were visually the same for all of the speeds tested using this design; the results only differed in the resulting velocity values obtained.

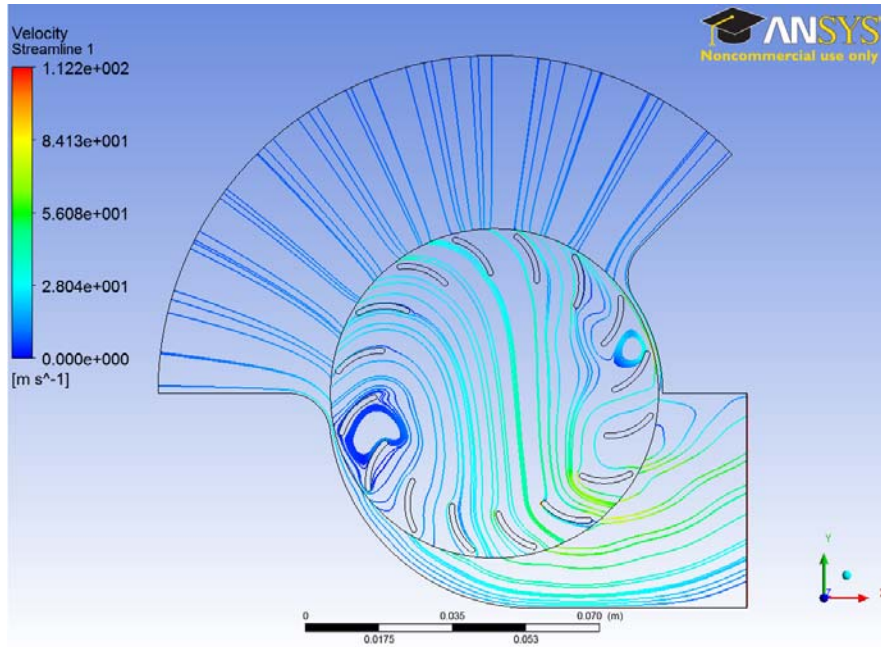


Figure 23. Air velocity streamlines in CFF operating at 8,000 rpm

C. ANALYTICAL VERSUS EXPERIMENTAL RESULTS

The comparison between the CFF's actual performance and the analytically determined performance was made by comparing the thrust generation, outlet velocity and power consumption. The comparison of the resulting velocities is most crucial because both power and thrust are functions of velocity, so the analytical formulation of thrust and power are calculated from the predicted outlet velocity. Therefore; for a more complete comparison of the analytical and experimental models the methods for measuring thrust and power were independent of the fan's measured outlet velocity.

1. Thrust

Figure 24 shows the comparison of the analytically determined thrust and the experimental thrust as measured by the tri-beam balance. The analytical thrust was found by multiplying the ANSYS CFX solutions for mass flow rate and outlet velocity. Table 3 lists the values of mass flow rate and velocities used, as well as the resulting thrust calculation. Table 4 lists the measured thrust from the experimental model at 12 points throughout the operational speed range.

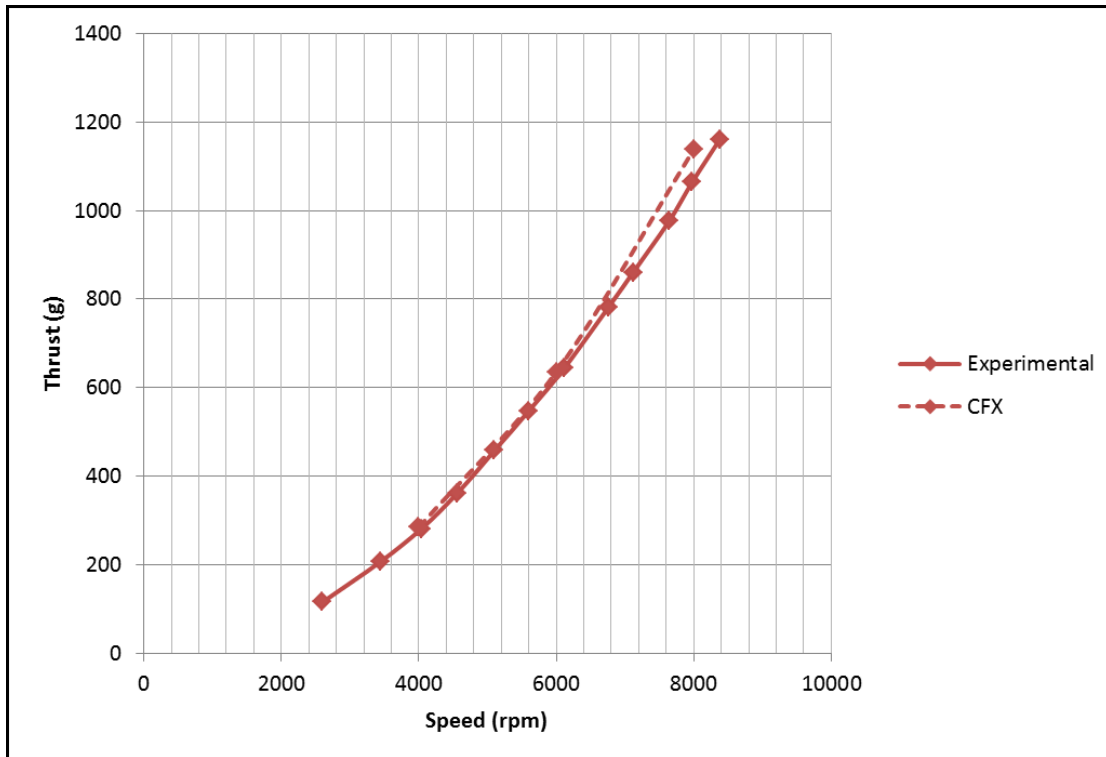


Figure 24. Experimental and analytical thrust calculations

Figure 24 shows that the experimental thrust measurements and analytically determined thrust match well over the entire CFF operating range, with a maximum error of 6.4% at the maximum operating speed of 8,000 rpm.

Table 3. ANSYS CFX data for analytical thrust calculation

Speed (rpm)	Mass Flow Rate (kg/s)	Outlet Velocity (m/s)	Thrust (g)
4000	0.147665	18.9444	285.1601
6000	0.21851	28.5411	635.7293
8000	0.290615	38.4289	1138.432

Table 4. Thrust measurements from CFF test rig

Speed (rpm)	Thrust (g)
2600	116
3440	207
4040	282
4560	362
5100	458
5600	548
6120	645
6760	782
7120	861
7640	976
7980	1065
8380	1161

2. Velocity Profiles

The CFF outlet velocity was determined using pressure sensing probes at the fan's outlet plane. Thirty samples were taken at 0.1 second intervals and those samples were averaged to determine the pressure at each sensed point. Negative pressures were recorded along some of the edges of the outlet plane indicating that flow in these regions was recirculating, forming eddies. Because negative pressure readings do not give useful velocity information, all of the negative pressures were set to zero. Then Equation 9 was used to determine the velocity at each sensed point. Tables 5, 6 and 7 list the outlet plane velocities at CFF rotor speeds of 4,000, 6,000 and 8,000 rpm, respectively.

Table 5. Velocity measurements from grid probe, 4,000 rpm (m/s)

	Span (One Inch Spacing)							
	Width (Half Inch Spacing)	0.00	22.58	24.15	20.96	20.58	23.90	24.23
0.00		20.71	23.00	18.57	18.20	23.30	21.40	0.00
0.00		17.73	19.63	14.53	12.81	19.54	17.36	0.00
0.00		14.27	16.77	8.79	7.45	0.00	12.74	0.00

Table 6. Velocity measurements from grid probe, 6,000 rpm (m/s)

	Span (One Inch Spacing)							
Width (Half Inch Spacing)	0.00	33.59	36.20	32.07	30.56	35.86	36.10	0.00
	0.00	29.92	34.36	28.56	26.87	34.93	31.17	0.00
	0.00	24.75	28.73	22.50	19.12	29.10	25.18	0.00
	0.00	18.83	23.03	13.35	7.66	7.90	18.10	0.00

Table 7. Velocity measurements from grid probe, 8,000 rpm (m/s)

	Span (One Inch Spacing)							
Width (Half Inch Spacing)	0.00	45.37	47.97	42.38	41.38	48.06	48.82	0.00
	0.00	41.07	45.74	37.37	36.93	47.57	42.13	0.00
	0.00	34.15	38.84	28.20	26.66	40.03	33.95	0.00
	0.00	25.70	31.18	13.44	11.70	13.74	23.61	0.00

The experimental data in Figure 25 was developed by averaging the velocity data across the span of the rotor. The zero values for velocity at the ends of the rotor were not included in these calculations because, by using symmetry planes, the analytical model did not experience any wall effects in the span direction. Figure 25 compares the experimental and analytical velocities and three rotor speeds. The figure shows that the increase in outlet velocity as rotor speed increased was consistent between the analytical model and the experiment, and the decrease in velocity across the width is also consistent.

The velocity profiles in Figure 25 all had the same general shape, regardless of the speed that the CFF was operating, so 8,000 rpm was selected to conduct a more detailed velocity analysis using the CFF test rig. To more easily visualize the velocity profile at the fan's outlet, Figure 26 was developed by plotting all of the velocity data in Table 7. This figure shows that there was a large variation in data across the span of the rotor, instead of the expected constant velocity near the center of span where the effects of the walls at the housing ends should be minimal. The resulting uncertainty led to the development of the rake probe to more accurately construct the velocity profile.

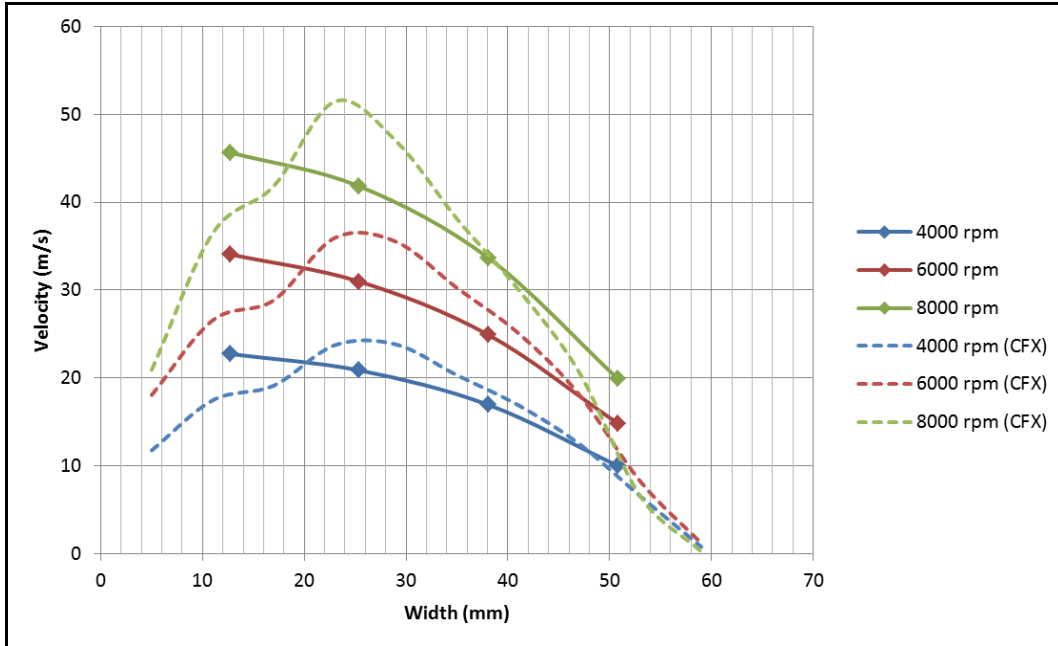


Figure 25. Comparison of experimental to analytical outlet velocity

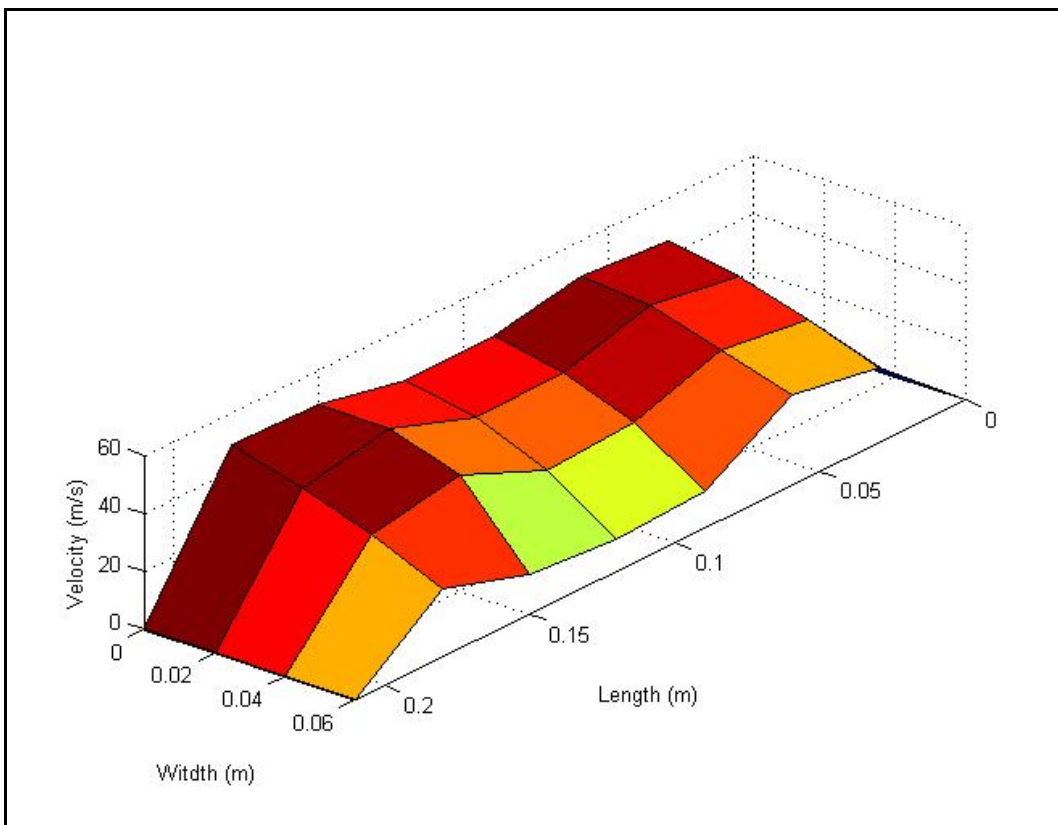


Figure 26. Outlet velocity profile using grid probe, 8,000 rpm

The pressure sensing rake probe was used to collect the data used to generate Figure 27. The data manipulation was the same as described for the generation of the preceding plots. The velocity information used to generate the surface plot in Figure 27 is tabulated in Appendix D. Figure 27 greatly clarifies the previously unresolved outlet velocity profile. The effects that the side walls had on the outlet velocity was expected, but significant reduction in the mid-span velocity due to the blade support disk (Figure 11) was unanticipated. The reduction in velocity in this region is what causes the experimental velocities to be less than the predicted velocity profile. The symmetry planes used in the ANSYS CFX model resulted in an undisturbed approximation of flow in a theoretical infinite rotor. Figure 27 shows that the one-quarter span and three-quarter span locations are the closest representations of undisturbed flow at the outlet plane, and that instead of an average velocity profile, the velocity profiles at these locations should be used to compare to the analytical results.

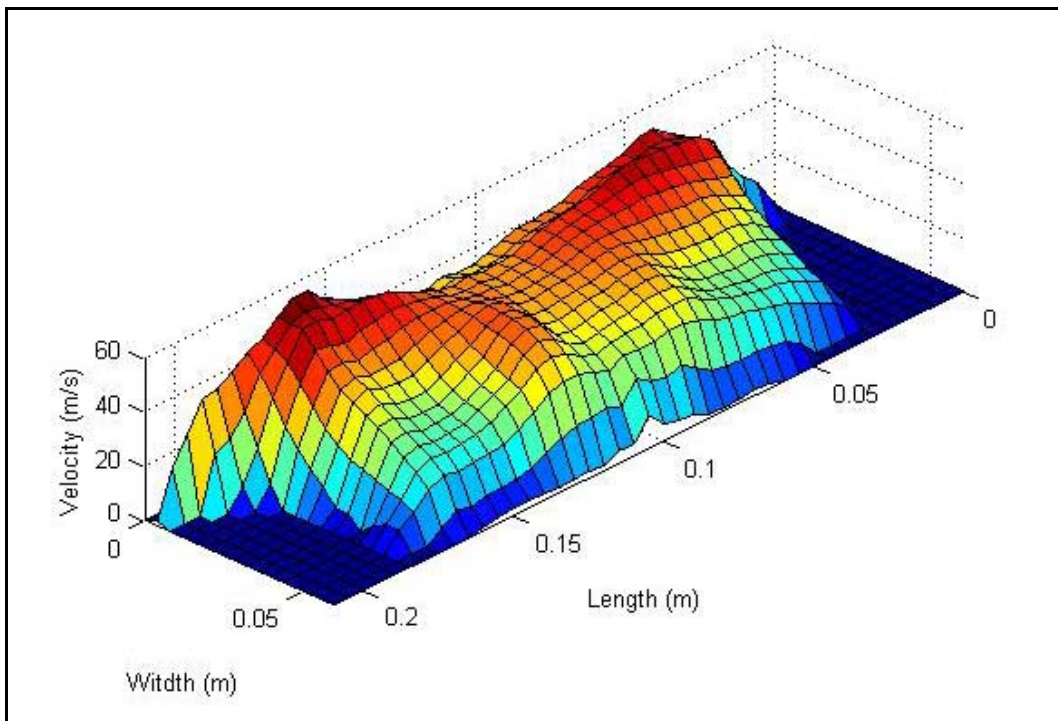


Figure 27. Outlet velocity profile using rake probe, 8,000 rpm

Figure 28 is a plot of the analytical exit-plane velocity and the experimental velocity profile obtained at the three-quarter span location. The plots have the same basic shape but the experimental data is spread over a larger width than the analytical. This difference is due to the pressure sensing ports being located 20 mm from the actual exit plane of the CFF housing. This location was necessary because locating the pressure port mounting plate too close to the fan's outlet caused the fan to transition in and out of stall, which in turn caused severe pressure fluctuations making data collection impossible. The added distance of exit flow to the pressure ports allowed for external air to be entrained in the flow, thereby giving a seeming wider total width. The maximum exit velocity found experimentally was 56.36 m/s, and the maximum analytically determined exit velocity was 51.87 m/s. This comparison yielded a 7.97% error.

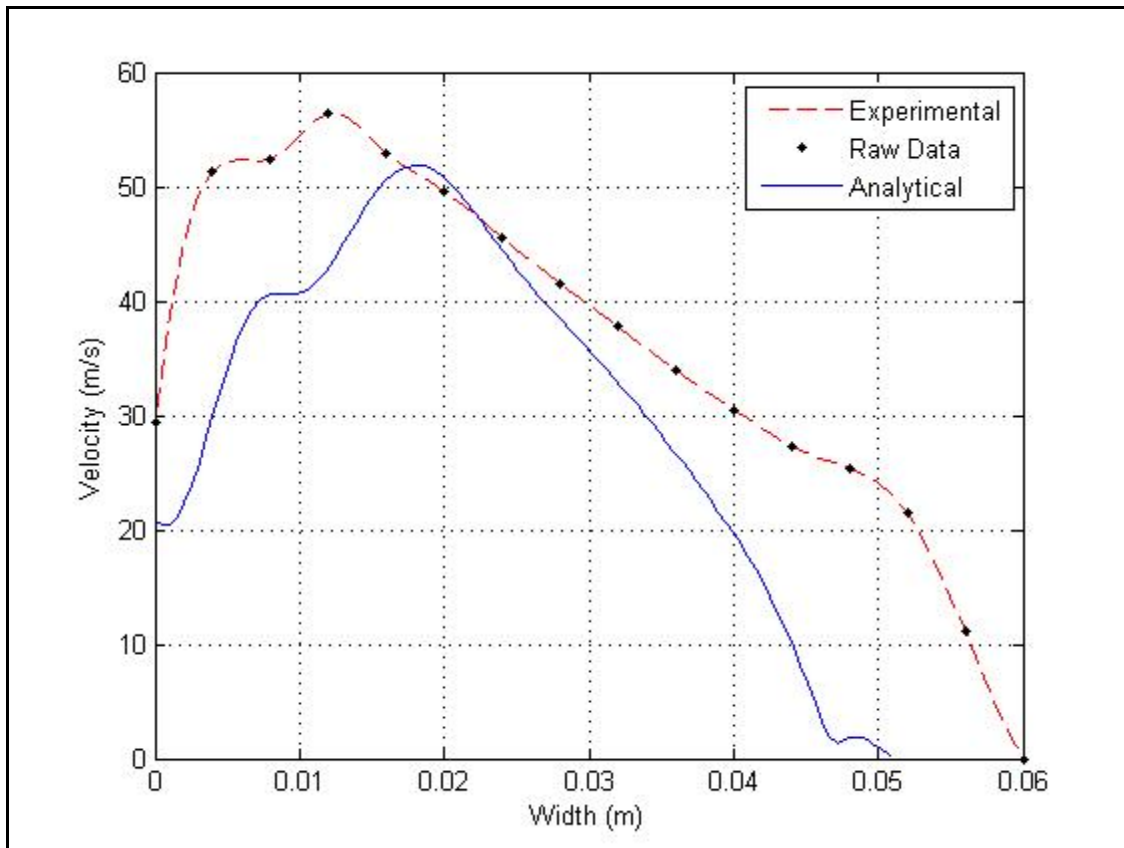


Figure 28. Comparison of experimental and analytical velocity profiles from experimental fine mesh data

3. Power

The analytically determined and experimentally measured CFF power can be seen in Figure 29. This figure shows that for rotor speeds up to 6,000 rpm, the power can be accurately predicted by the ANSYS model. As the rotational velocity was increased above 6,000 rpm, the error between actual and predicted power grew rapidly. The divergence between predicted and actual power is explained by the drop in CFF efficiency at speeds greater than 6,000 rpm, as described by Antoniadis [6] in his CFF performance research.

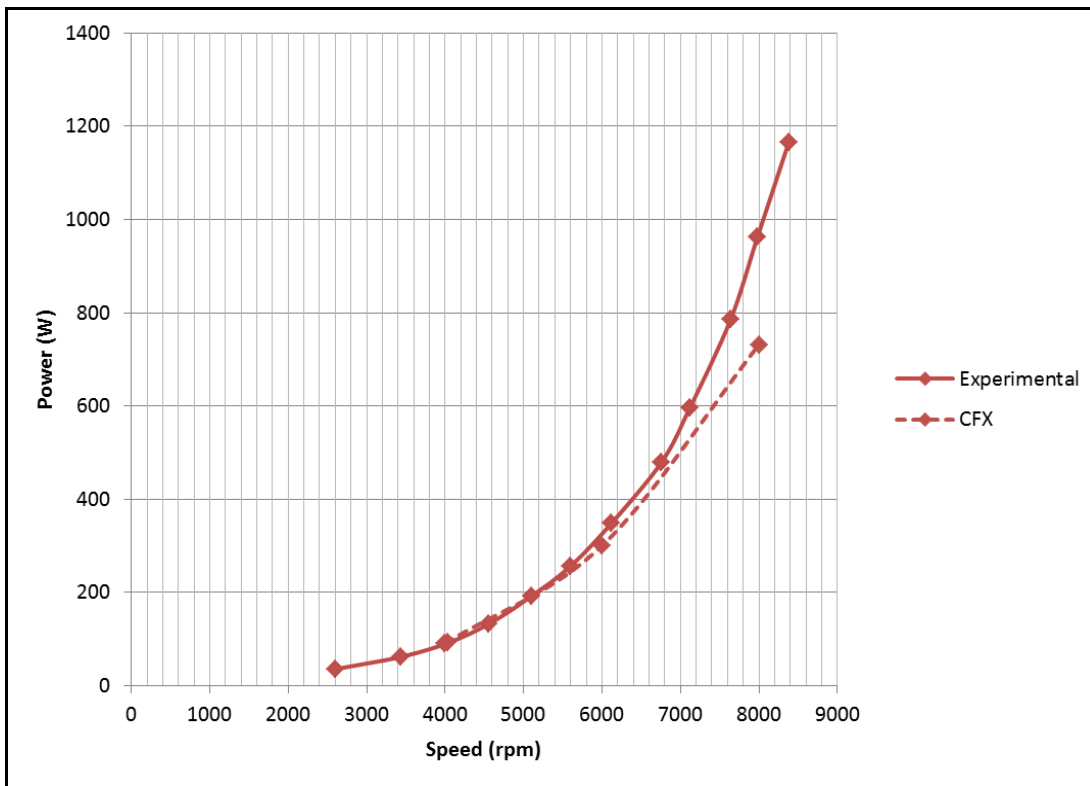


Figure 29. Experimental and analytical power calculations

THIS PAGE INTENTIONALLY LEFT BLANK

V. CONCLUSION AND RECOMMENDATIONS

A. THRUST TO WEIGHT RATIO

This propulsion system requires maximum thrust during take-off and landing, therefore the CFF will need to operate at the highest speed possible to generate this thrust. As the vehicle transitions to level flight, then the speed can be reduced to operate the CFF more efficiently. The maximum speed of operation for this assembly was 8,000 rpm, which resulted in a generated thrust of approximately 1,065 grams. The entire CFF assembly, without a prime mover, weighs 377 grams, which results in a thrust-to-weight ratio of 2.825. The resulting ratio is an optimistic result, as vertical take-off only requires that the thrust-to-weight ratio be greater than one.

The initial vision for powering the CFF was to use an electric motor powered from lithium polymer (LiPo) batteries. To generate the 1 KW of electrical power required, an initial configuration was assembled consisting of a motor weighing 352 grams, a motor controller weighing 192 grams, and a six-cell LiPo battery pack weighing 807 grams. This setup did provide sufficient power for CFF operation, but with a combined weight of 1,729 grams, the thrust-to-weight ratio was reduced to 0.616. Another obstacle using this design is that the single battery pack is only capable of powering the CFF for approximately six minutes.

B. HOUSING AND ROTOR DESIGN

The most important result from the housing design investigation was realizing the accuracy with which ANSYS CFX predicted the performance of the model. The ability to relatively quickly evaluate a number of different designs saved countless hours of the fabrication and experiment that would be required without the aid of computer modeling. The housing that was selected and constructed performed almost exactly as the computational model predicted. The housing shape performed well over a wide range of speeds, so it is an ideal candidate for a VTOL aircraft.

The carbon-fiber rotor was selected based upon its rated speed and light weight. As described above, the rotor and housing combination was accurately modeled by

ANSYS CFX and performed well, but this off-the-shelf design is likely not ideal to maximize thrust. Antoniadis [6] found in his research on varying blade configurations, that a 22-blade rotor with a slightly different blade profile should operate more efficiently and produce a greater thrust-to-power ratio.

C. RECOMMENDATIONS

Power generation is the most significant obstacle is the current design. The added weight of a sufficiently sized motor combined with an adequate number of battery cells to power the motor makes this design infeasible. There are a number of different design modifications that should be investigated to overcome this obstacle.

An electric motor is not sufficient to power the current assembly with no modifications. An alternative to an electric motor would be to use a gasoline powered engine instead. Small engines like those found in remote controlled (RC) airplanes are capable of operating at all of the speeds investigated in this study and provide twice the power of an electric motor at only half of the total weight. The noise produced by a gas engine is not a concern for the current design because of the already loud operation of the CFF.

There are a number of other design investigations that should be performed either instead of motor replacement or in conjunction with it. During this project ANSYS CFX proved to be an invaluable tool for predicting the CFF performance. The housing developed in this thesis should be investigated analytically with a number of different variations. The development of a new rotor would likely improve the overall performance. The rotor's blade count, blade angle, diameter and span should be analyzed to determine the optimal rotor configuration to use with the current housing. The proposed housing design could be easily scaled to accommodate virtually any rotor design. Modifications to the housing should also be investigated. Physically the housing can be altered for a lighter design by removing extra material on the endplates that has no structural significance. Additionally, constructing the housing out of carbon fiber vice aluminum would constitute an immediate 55.6% weight savings. Finally, thrust augmentation through the use of multiple rotors or outlet nozzles should be analyzed.

APPENDIX A. ASSEMBLY DESIGN PROCESS

A. ROTOR SELECTION

The initial rotor selected for CFF design was a 12-inch span, 1.25-inch diameter, aluminum rotor from the DFA32 series DC cross-flow fan manufactured by SOFASCO. Figure 30 shows this fan rotor after removal from the factory housing.



Figure 30. DFA32 series DC CFF rotor

This CFF was first tested in its original casing to determine the amount of thrust it was capable of producing prior to modification. The CFF was designed to provide cooling for electrical components, and had a rated speed of about 1,000 rpm. To produce thrust for propulsion, much higher rotational speeds were required, so the fan was tested up to 8,000 rpm. Following the initial testing, this rotor design was abandoned for two reasons. When the CFF was operating at the maximum speed of 8,000 rpm, the fan produced 95 grams of thrust which when compared to the CFF's weight of 289 grams did not seem like a reasonable candidate for augmentation. The second reason for discontinued interest in this design was the extreme deflection of the rotor blades during

high speed operation. ANSYS STRUCTURAL was used to model this rotor at speeds in excess of 8,000 rpm. Figure 31 shows the results of the safety factor investigation performed at 10,000 rpm. At this speed, the minimum safety factor found was 0.803, which indicated a probable rotor failure at this speed. Destructive testing was planned to verify the ANSYS results, but the test was stopped with no failure at 9,100 rpm due to the rotor bow causing rubbing between the rotor and housing.

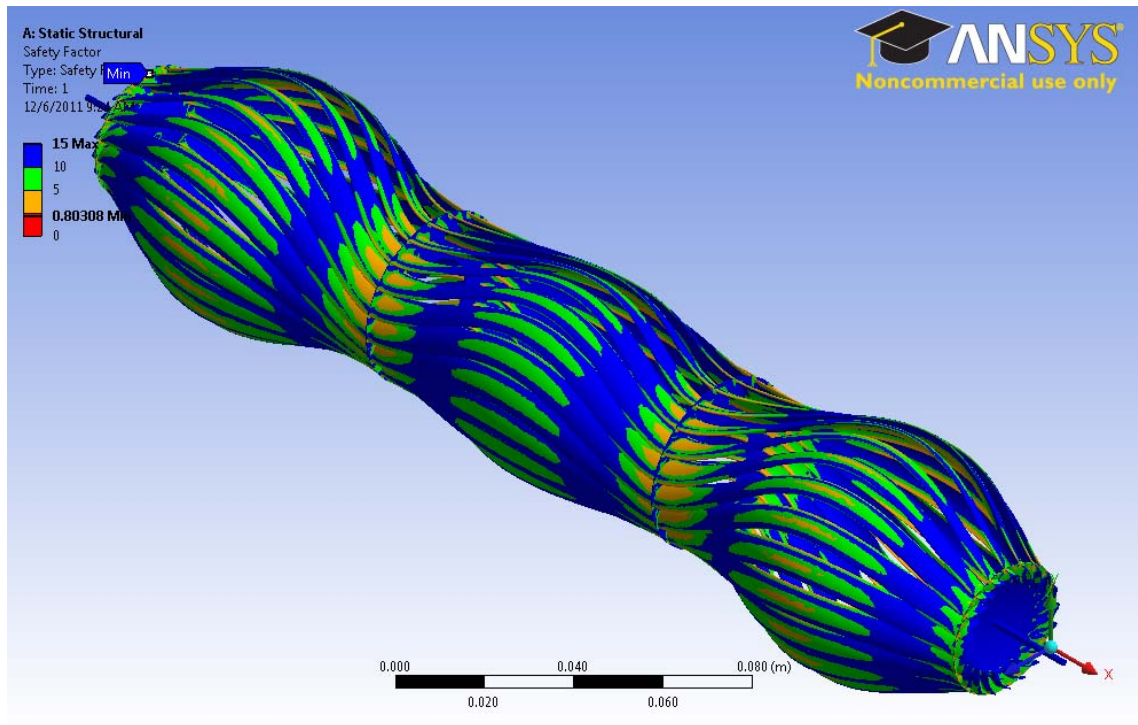


Figure 31. ANSYS STRUCTURAL safety factor investigation of rotor at 10,000 rpm

After the aluminum rotor concept was abandoned, the carbon fiber rotor was identified as the next reasonable rotor design for this project. A detailed structural analysis of the new rotor was not conducted due to the rotor coming from the manufacturer with a designed speed of 8,000 rpm. One initial test of this rotor was conducted to verify that it operated at 8,000 rpm with no apparent structural flaws. Upon successful completion of this test, it was adopted as the rotor that would be used to design a CFF housing around. Structural analysis should be performed on this rotor if tests in excess of 8,000 rpm will be conducted in the future.

B. HOUSING DESIGN

The design of an appropriate housing was a highly iterative process. To begin, an exceptionally simple design was conceived, so that a gross understanding of the flow through the CFF could be attained. The simple design would also be easy to fabricate if the computational analysis results warranted further experimentation with the design. Figure 32 shows the initial design and the resulting velocity streamlines following CFD analysis at 8,000 rpm.

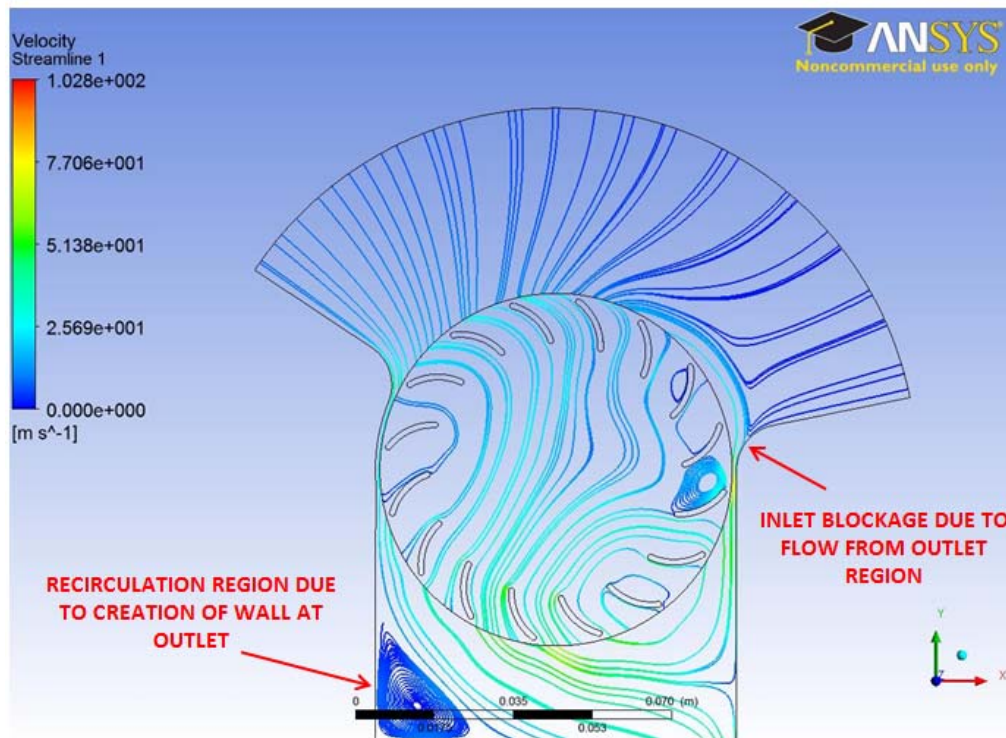


Figure 32. Velocity streamlines through initial housing design

Two significant problems were identified after the analysis of this design. The first can be seen in the lower left corner of the streamline image. In this area, ANSYS CFX built a wall covering the outlet, because the results of the CFD calculations being performed indicated that flow should be entering through the outlet plane. Because the exit was defined as an outlet, ANSYS changed the outlet to a wall to prevent inflow. The second problem can be seen above the rotor at the right side of the inlet. The vortex formed in the rotor was entraining flow and carrying flow from the high pressure outlet,

around the blade tips, and back to the inlet side of the rotor. This blocked the inlet flow into the rotor and consequently, only about two thirds of the rotor's inlet surface area was being used.

The streamline flow through this model led directly to the development of a second model. A second housing was designed based on the resulting flow lines in the first housing. Figure 33 shows the second housing design. This design is also shown with the calculated velocity streamlines. Unfortunately, this housing performed no better than the first and had the same two inherent flaws.

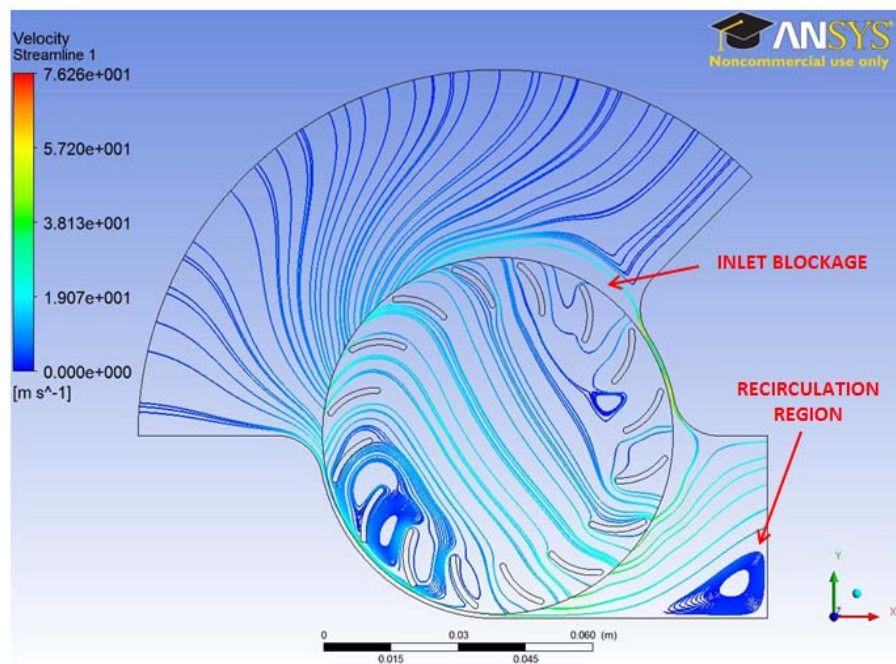


Figure 33. Velocity streamlines through the second proposed housing

The design process was continued by slowly manipulating the second model, one feature at a time, and rerunning the analysis. In total, eleven models were analyzed to find that the blade tip leakage problem was corrected by adding a corner to the housing profile where the right side of the rotor meets the housing, and that by allowing flow to leave the rotor earlier, into a large radius, the air was directed toward the outlet instead of at the upward angle seen above. This solved the issue of flow recirculation at the outlet plane.

APPENDIX B. ANSYS CFX SETTINGS AT 8,000 RPM

Analysis Type	<p>Basic Settings</p> <ul style="list-style-type: none"> • External Solver Coupling <ul style="list-style-type: none"> ○ Option: None • Analysis Type <ul style="list-style-type: none"> ○ Option: Transient • Time Duration <ul style="list-style-type: none"> ○ Option: Total Time ○ Total Time: 0.0375 [s] • Time Steps <ul style="list-style-type: none"> ○ Option: Timesteps ○ Timesteps: 2.08e-005 [s] • Initial Time <ul style="list-style-type: none"> ○ Option: Automatic with Value ○ Time: 0 [s]
Rotor	<p>Basic Settings</p> <ul style="list-style-type: none"> • Location & Type <ul style="list-style-type: none"> ○ Location: B305 ○ Domain Type: Fluid Domain ○ Coordinate Frame: Coord 0 • Fluid and Particle Definitions <ul style="list-style-type: none"> ○ Fluid 1 <ul style="list-style-type: none"> ▪ Option: Material Library ▪ Material: Air Ideal Gas ▪ Morphology <ul style="list-style-type: none"> • Option: Continuous Fluid ▪ Minimum Volume Fraction: unchecked • Domain Models <ul style="list-style-type: none"> ○ Pressure <ul style="list-style-type: none"> ▪ Reference Pressure: 1 [atm] ○ Buoyancy Model <ul style="list-style-type: none"> ▪ Option: Non Buoyant ○ Domain Motion <ul style="list-style-type: none"> ▪ Option: Rotating ▪ Angular Velocity: 8000 [rev min⁻¹] ○ Axis Definition <ul style="list-style-type: none"> ▪ Option: Coordinate Axis ▪ Rotation Axis: Global Z ○ Mesh Deformation <ul style="list-style-type: none"> ▪ Option: None <p>Fluid Models</p> <ul style="list-style-type: none"> • Heat Transfer <ul style="list-style-type: none"> ○ Option: Total Energy ○ Incl. Viscous Work Term: Checked • Turbulence <ul style="list-style-type: none"> ○ Option: k-Epsilon ○ Wall Function: Scalable ○ High Speed (compressible): Unchecked ○ Turbulent Flux Closure for HT: Unchecked • Combustion <ul style="list-style-type: none"> ○ Option: None

	<ul style="list-style-type: none"> • Thermal Radiation <ul style="list-style-type: none"> ○ Option: None • Electromagnetic Model: Unchecked <p>Initialization</p> <ul style="list-style-type: none"> • Domain Initialization <ul style="list-style-type: none"> ○ Frame Type: Rotating ○ Coord Frame: Unchecked • Initial Conditions <ul style="list-style-type: none"> ○ Velocity Type: Cylindrical ○ Cylindrical Velocity Components <ul style="list-style-type: none"> ▪ Option: Automatic with Value ▪ Axial Component: 0 [m s⁻¹] ▪ Radial Component: 0 [m s⁻¹] ▪ Theta Component: 0 [m s⁻¹] • Static Pressure <ul style="list-style-type: none"> ○ Option: Automatic with Value ○ Relative Pressure: 1 [Pa] • Temperature <ul style="list-style-type: none"> ○ Option: Automatic with Value ○ Temperature: 288.15 [K] • Turbulence <ul style="list-style-type: none"> ○ Option: Medium (Intensity = 5%) 	
Rotor	Rotor Default	<p>Basic Settings</p> <ul style="list-style-type: none"> • Boundary Type: Wall <ul style="list-style-type: none"> ○ Location: (automatically fills out) ○ Coord Frame: Unchecked ○ Frame Type: Rotating <p>Boundary Details</p> <ul style="list-style-type: none"> • Mass and Momentum <ul style="list-style-type: none"> ○ Option: No Slip Wall ○ Wall Velocity: Unchecked • Wall Roughness <ul style="list-style-type: none"> ○ Option: Smooth Wall • Heat Transfer <ul style="list-style-type: none"> ○ Option: Adiabatic <p>Sources</p> <ul style="list-style-type: none"> • Boundary Source: Unchecked
Rotor	Symmetry	<p>Basic Settings</p> <ul style="list-style-type: none"> • Boundary Type: Symmetry • Location: RototSym1 RotorSym2
Housing	Basic Settings	<ul style="list-style-type: none"> • Location & Type <ul style="list-style-type: none"> ○ Location: B665 ○ Domain Type: Fluid Domain ○ Coordinate Frame: Coord 0 • Fluid and Particle Definitions... <ul style="list-style-type: none"> ○ Fluid 1 <ul style="list-style-type: none"> ▪ Option: Material Library ▪ Material: Air Ideal Gas

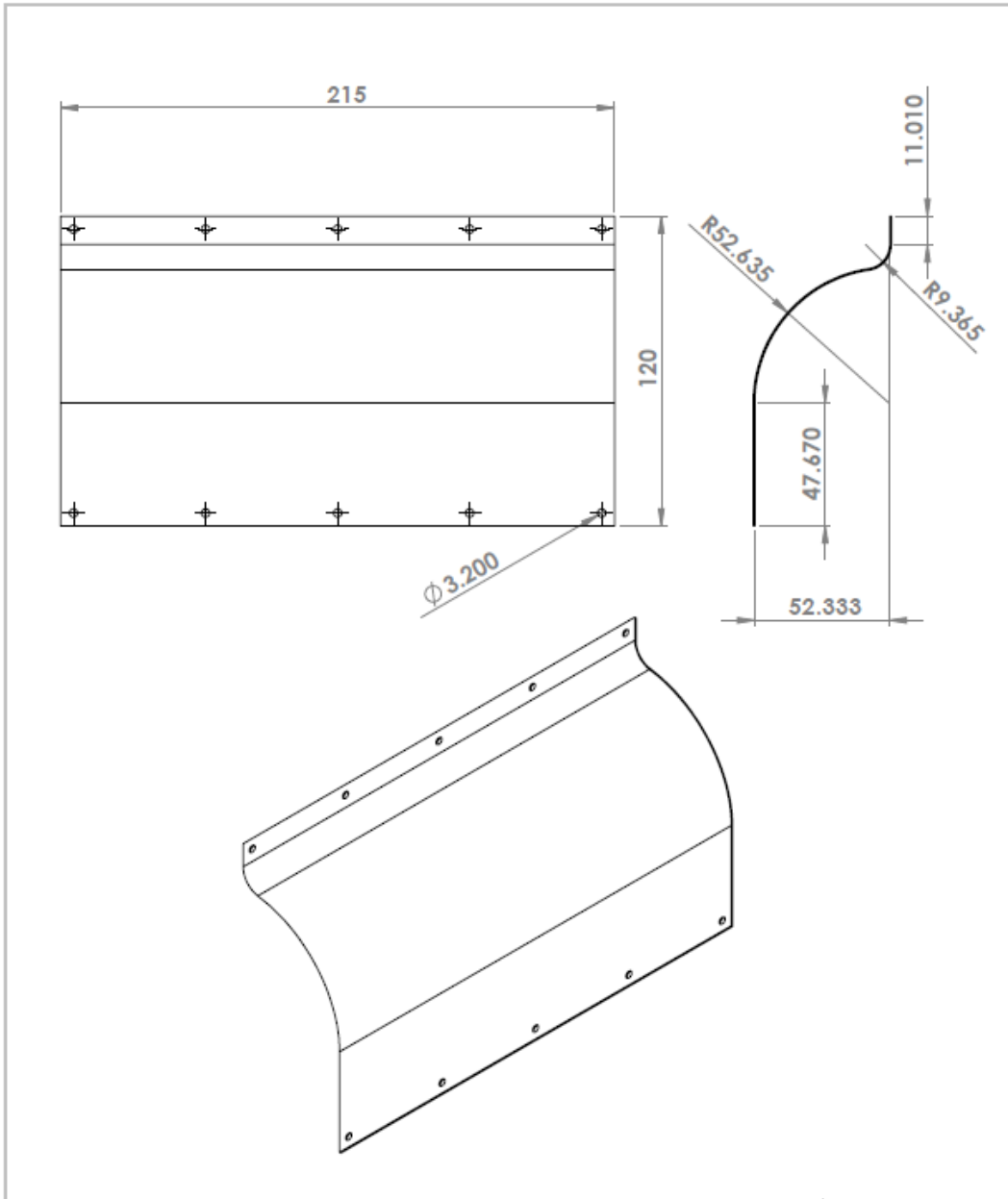
	<ul style="list-style-type: none"> <ul style="list-style-type: none"> <ul style="list-style-type: none"> ▪ Morphology <ul style="list-style-type: none"> • Option: Continuous Fluid ▪ Minimum Volume Fraction: Unchecked • Domain Models <ul style="list-style-type: none"> ○ Pressure <ul style="list-style-type: none"> ▪ Reference Pressure: 1 [atm] ○ Buoyancy Model <ul style="list-style-type: none"> ▪ Option: Non Buoyant ○ Domain Motion <ul style="list-style-type: none"> ▪ Option: Stationary ○ Mesh Deformation <ul style="list-style-type: none"> ▪ Option: None Fluid Models <ul style="list-style-type: none"> • Heat Transfer <ul style="list-style-type: none"> ○ Option: Total Energy ○ Incl. Viscous Work Term: Checked • Turbulence <ul style="list-style-type: none"> ○ Option: k-Epsilon ○ Wall Function: Scalable ○ High Speed (compressible): Unchecked ○ Turbulent Flux Closure for HT: Unchecked • Combustion <ul style="list-style-type: none"> ○ Option: None • Thermal Radiation <ul style="list-style-type: none"> ○ Option: None • Electromagnetic Model: Unchecked Initialization <ul style="list-style-type: none"> • Domain Initialization: <ul style="list-style-type: none"> ○ Coord Frame: Unchecked • Initial Conditions <ul style="list-style-type: none"> ○ Velocity Type: Cylindrical ○ Cylindrical Velocity Components <ul style="list-style-type: none"> ▪ Option: Automatic with Value ▪ Axial Component: 0 [m s⁻¹] ▪ Radial Component: 0 [m s⁻¹] ▪ Theta Component: 0 [m s⁻¹] ○ Velocity Scale: Unchecked • Static Pressure <ul style="list-style-type: none"> ○ Option: Automatic with Value ○ Relative Pressure: 1 [Pa] • Temperature <ul style="list-style-type: none"> ○ Option: Automatic with Value ○ Temperature: 288.15 [K] • Turbulence <ul style="list-style-type: none"> ○ Option: Medium (Intensity = 5%) 		
Housing	<table border="1" style="width: 100%; border-collapse: collapse;"> <tr> <td style="width: 25%; text-align: center;">Housing Default</td> <td style="width: 75%;"> Basic Settings <ul style="list-style-type: none"> • Boundary Type: Wall <ul style="list-style-type: none"> ○ Location: (automatically fills out) ○ Coord Frame: Unchecked Boundary Details <ul style="list-style-type: none"> • Mass and Momentum <ul style="list-style-type: none"> ○ Option: No Slip Wall ○ Wall Velocity: Unchecked </td> </tr> </table>	Housing Default	Basic Settings <ul style="list-style-type: none"> • Boundary Type: Wall <ul style="list-style-type: none"> ○ Location: (automatically fills out) ○ Coord Frame: Unchecked Boundary Details <ul style="list-style-type: none"> • Mass and Momentum <ul style="list-style-type: none"> ○ Option: No Slip Wall ○ Wall Velocity: Unchecked
Housing Default	Basic Settings <ul style="list-style-type: none"> • Boundary Type: Wall <ul style="list-style-type: none"> ○ Location: (automatically fills out) ○ Coord Frame: Unchecked Boundary Details <ul style="list-style-type: none"> • Mass and Momentum <ul style="list-style-type: none"> ○ Option: No Slip Wall ○ Wall Velocity: Unchecked 		

		<ul style="list-style-type: none"> • Wall Roughness <ul style="list-style-type: none"> ○ Option: Unchecked • Heat Transfer <ul style="list-style-type: none"> ○ Option: Adiabatic Sources <ul style="list-style-type: none"> • Boundary Source: Unchecked
Housing	Inlet	Basic Settings <ul style="list-style-type: none"> • Boundary Type: Opening • Location: Inlet • Coord Frame: Unchecked Boundary Details <ul style="list-style-type: none"> • Flow Regime <ul style="list-style-type: none"> ○ Option: Subsonic • Mass and Momentum <ul style="list-style-type: none"> ○ Option: Op. Pres. and Dirn ○ Relative Pressure: 0 [Pa] • Flow Direction <ul style="list-style-type: none"> ○ Option: Normal to BC • Loss Coefficient: Unchecked • Turbulence <ul style="list-style-type: none"> ○ Option: Medium • Heat Transfer <ul style="list-style-type: none"> ○ Option: Static Temperature ○ Static Temperature: 288.15 [K] Sources <ul style="list-style-type: none"> • Boundary Source: Unchecked
Housing	Outlet	Basic Settings <ul style="list-style-type: none"> • Boundary Type: Outlet • Location: Outlet • Coord Frame: Unchecked Boundary Details <ul style="list-style-type: none"> • Flow Regime <ul style="list-style-type: none"> ○ Option: Subsonic • Mass And Momentum <ul style="list-style-type: none"> ○ Option: Average Static Pres. ○ Relative Pressure: 0 [Pa] ○ Pres. Profile Blend: 0.05 • Pressure Averaging <ul style="list-style-type: none"> ○ Option: Average Over Outlet Sources <ul style="list-style-type: none"> • Boundary Source: unchecked
Housing	Symmetry	Basic Settings <ul style="list-style-type: none"> • Boundary Type: Symmetry • Location: HousingSym1 HousingSym2
Interfaces	Housing to Rotor	Basic Settings <ul style="list-style-type: none"> • Interface Type: Fluid Flow • Interface Side 1 <ul style="list-style-type: none"> ○ Domain: Housing ○ Region List: HousingInterface • Interface Side 2 <ul style="list-style-type: none"> ○ Domain: Rotor ○ Region List: RotorInterface

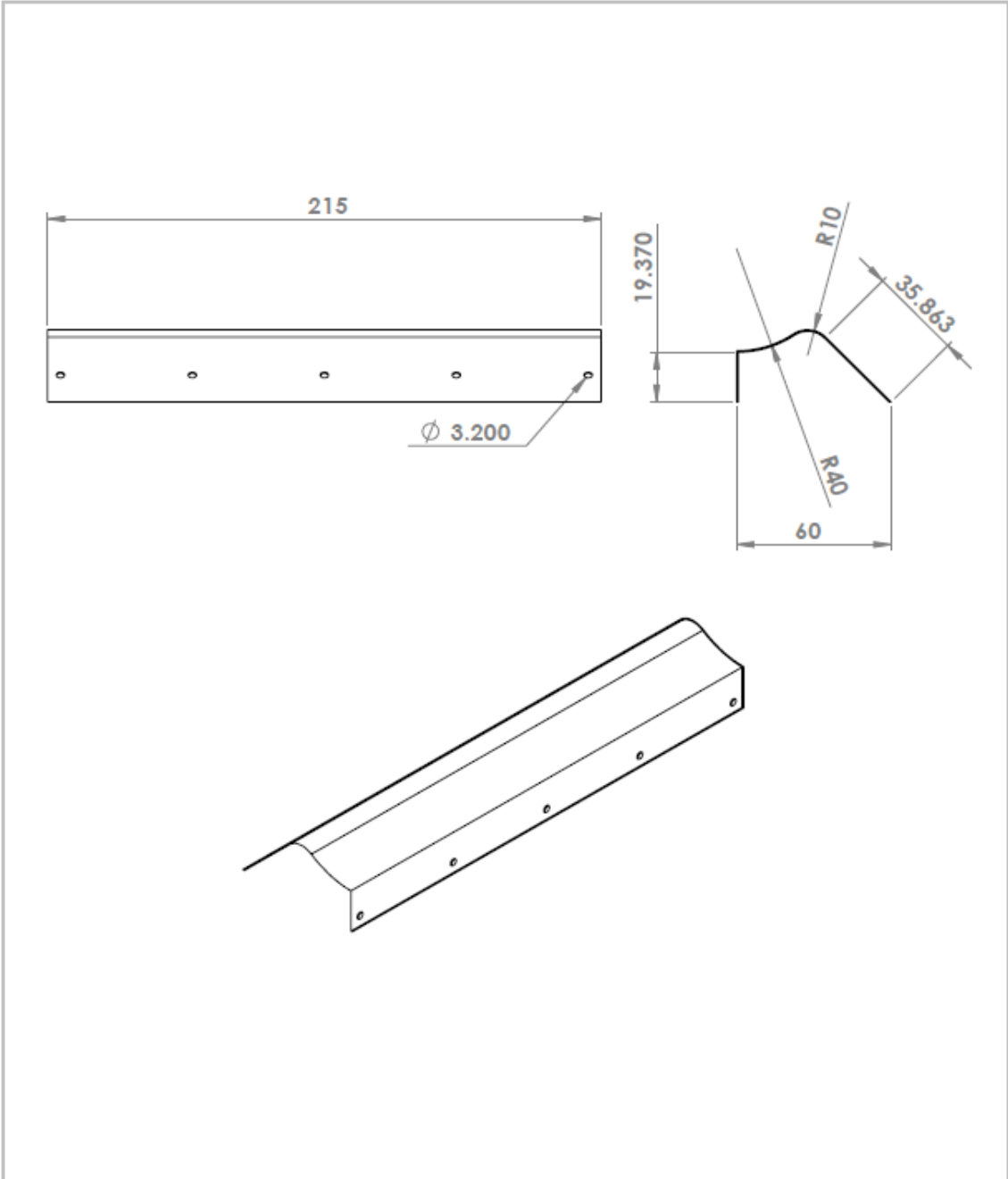
		<ul style="list-style-type: none"> • Interface Models <ul style="list-style-type: none"> ○ Option General Connection • Frame Change/ Mixing Model <ul style="list-style-type: none"> ○ Option Trans Rotor Stator • Pitch Change <ul style="list-style-type: none"> ○ Automatic <p>Additional Interface Models</p> <ul style="list-style-type: none"> • Mass and Momentum <ul style="list-style-type: none"> ○ Option Conservative Interface Flux • Interface Model <ul style="list-style-type: none"> ○ Option None • Conditional Connection Contrl Unchecked <p>Mesh Connection</p> <ul style="list-style-type: none"> • Mesh Connection <ul style="list-style-type: none"> ○ Option GGI • Intersection Control Unchecked
Solver	Solution Units	<p>Basic Settings</p> <ul style="list-style-type: none"> • Mass Units: [kg] • Length Units: [m] • Time Units: [s] • Temperature Units: [K] • Angle Units: CHECKED <ul style="list-style-type: none"> ○ Angle Units: [rad] • Solid Angle Units: CHECKED <ul style="list-style-type: none"> ○ Solid Angle Units: [sr]
Solver	Solver Control	<p>Basic Settings</p> <ul style="list-style-type: none"> • Advection Scheme <ul style="list-style-type: none"> ○ Option: High Resolution • Transient Scheme <ul style="list-style-type: none"> ○ Option: 2nd OrderBE • Timestep Initialization <ul style="list-style-type: none"> ○ Option: Automatic ○ Lower Courant Number: Unchecked ○ Upper Courant Number: Unchecked • Turbulence Numerics <ul style="list-style-type: none"> ○ Option: First Order • Convergence Control <ul style="list-style-type: none"> ○ Min. Coeff. Loops 1 ○ Max. Coeff. Loops 3 ○ Fluid Timescale Control <ul style="list-style-type: none"> ▪ Timescale Control: Coefficient Loops • Convergence Criteria <ul style="list-style-type: none"> ○ Residual Type: RMS ○ Residual Target: 1e-4 ○ Conservation Target: Unchecked • Elapsed Wall Clock Time Control: Unchecked • Interrupt Control: Unchecked <p>Equation Class Settings</p> <ul style="list-style-type: none"> • Equation Class: Continuity, • Continuity: Unchecked

		<p>Advanced Options</p> <ul style="list-style-type: none"> • Pressure Level Information: Unchecked • Body Forces: Unchecked • Interpolation Scheme: Unchecked • Temperature Damping: Unchecked • Velocity Pressure Coupling: Unchecked • Compressibility Control: Checked • High Speed Numerics: Checked • Total Pressure Option: Unchecked • Clip Pressure for Properties: Unchecked • Minimum Pressure for Properties: Unchecked • Intersection Control: Unchecked
Solver	Output Control	<p>Results</p> <ul style="list-style-type: none"> • Option: Standard • File Compression: Default • Output Equation Residuals: Unchecked • Extra Output Variable List: Unchecked <p>Backup Results: Blank</p> <p>Monitor</p> <ul style="list-style-type: none"> • Monitor Objects: Rotor Torque* Delta Mass Flow* Inlet Mass flow* Outlet Mass Flow* <p>*All objects are defined in expressions</p>

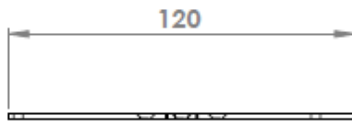
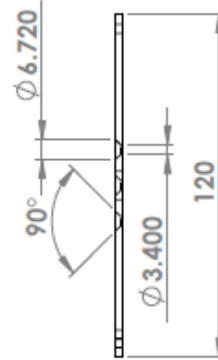
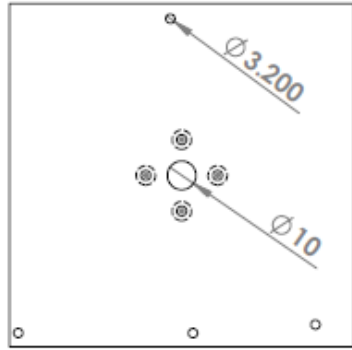
APPENDIX C. CFF COMPONENT DRAWINGS



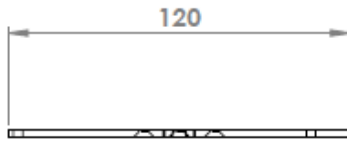
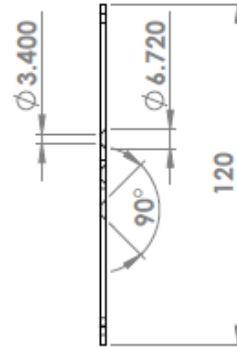
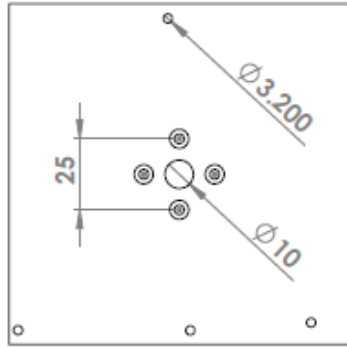
UNLESS OTHERWISE SPECIFIED: DIMENSIONS ARE IN MILLIMETERS		FINISH:		DEBUR AND BREAK SHARP EDGES		DO NOT SCALE DRAWING		REVISION	
SURFACE FINISH:									
TOLERANCES:									
LINEAR:									
ANGULAR:									
DRAWN	NAME	SIGNATURE	DATE			TITLE:			
CHKD						Housing Wall 1			
APPVD									
MFG									
Q.A									
				MATERIAL:		DWG NO.		A4	
				WEIGHT:		SCALE:1:5			SHEET 1 OF 1



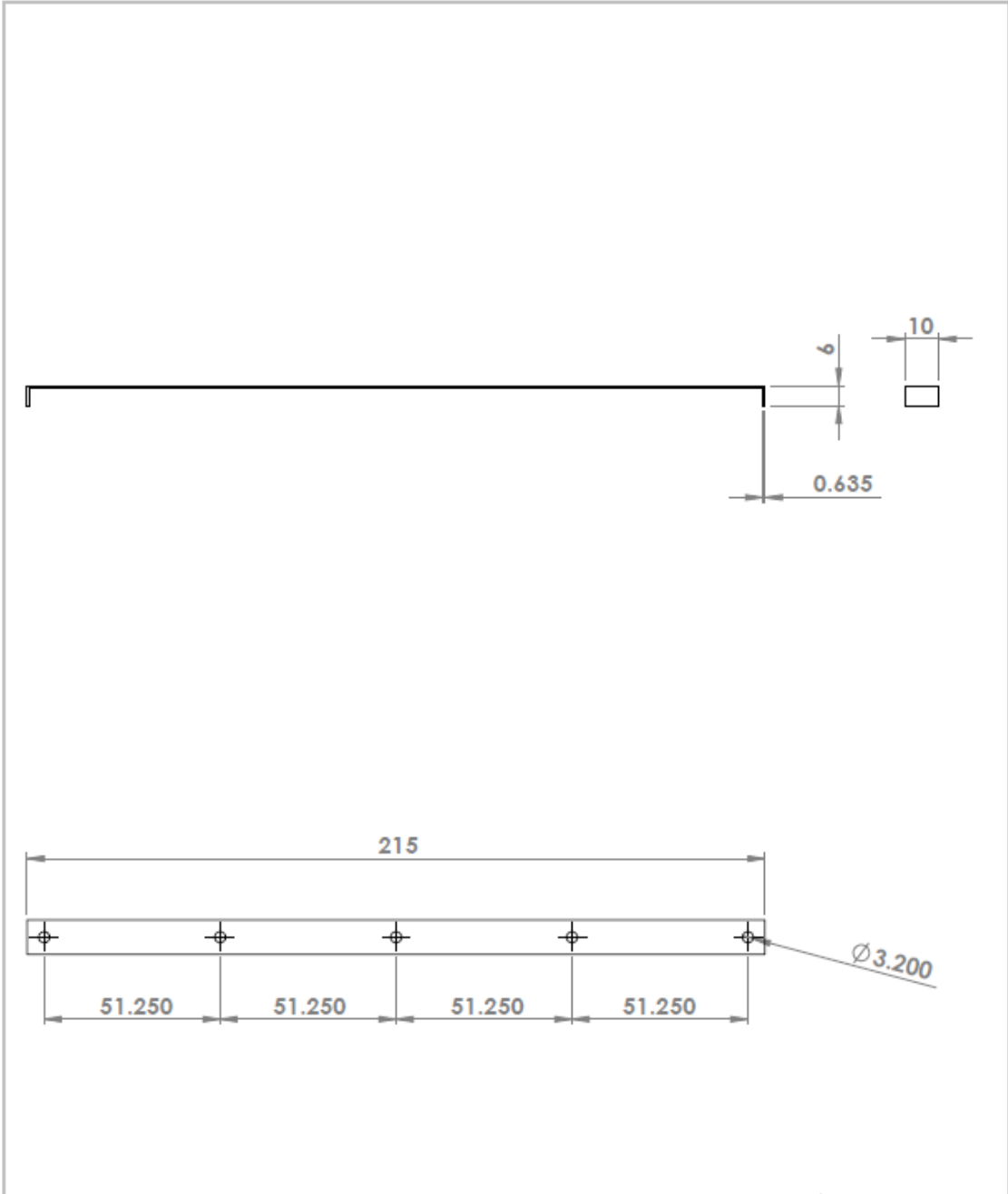
UNLESS OTHERWISE SPECIFIED: DIMENSIONS ARE IN MILLIMETERS		FINISH:		DEBUR AND BREAK SHARP EDGES		DO NOT SCALE DRAWING		REVISION	
SURFACE FINISH:									
TOLERANCES:									
LINEAR:									
ANGULAR:									
NAME		SIGNATURE		DATE		TITLE:			
DRAWN									
CHK'D									
APP'VD									
MFG									
Q.A						MATERIAL:		DWG NO. Housing Wall 2	
								A4	
						WEIGHT:		SCALE:1:5	
								SHEET 1 OF 1	



UNLESS OTHERWISE SPECIFIED: DIMENSIONS ARE IN MILLIMETERS		FINISH:		DEBUR AND BREAK SHARP EDGES		DO NOT SCALE DRAWING		REVISION	
SURFACE FINISH:									
TOLERANCES:									
LINEAR:									
ANGULAR:									
NAME		SIGNATURE		DATE		TITLE:			
DRAWN									
CHK'D									
APP'VD									
MFG									
Q.A				MATERIAL:		DWG NO.		A4	
						Motor End Plate			
				WEIGHT:		SCALE:1:2		SHEET 1 OF 1	

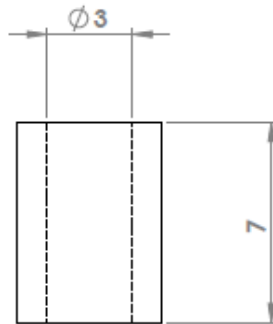
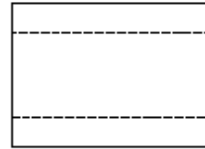
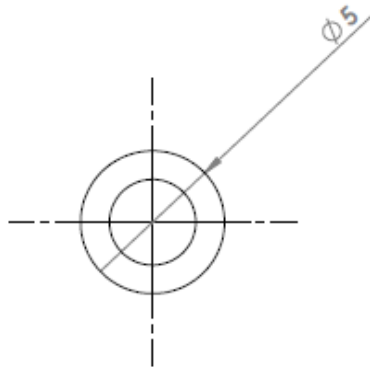


UNLESS OTHERWISE SPECIFIED: DIMENSIONS ARE IN MILLIMETERS		FINISH:		DEBUR AND BREAK SHARP EDGES		DO NOT SCALE DRAWING		REVISION	
SURFACE FINISH:									
TOLERANCES:									
LINEAR:									
ANGULAR:									
NAME		SIGNATURE		DATE		TITLE:			
DRAWN						Bearing End Plate A4			
CHK'D									
APP'VD									
MFG									
Q.A									
				MATERIAL:		DWG NO.			
						SCALE:1:2		SHEET 1 OF 1	
				WEIGHT:					

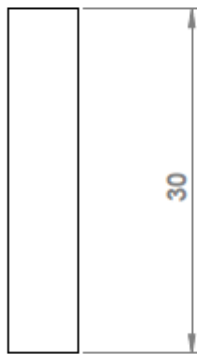
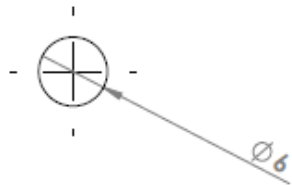


UNLESS OTHERWISE SPECIFIED: DIMENSIONS ARE IN MILLIMETERS		FINISH:		DEBUR AND BREAK SHARP EDGES		DO NOT SCALE DRAWING		REVISION	
SURFACE FINISH:									
TOLERANCES:									
LINEAR:									
ANGULAR:									
	NAME	SIGNATURE	DATE			TITLE:			
DRAWN									
CHK'D									
APP'VD									
MFG									
Q.A.									
				MATERIAL:		DWG NO.		A4	
				WEIGHT:		SCALE:1:2		SHEET 1 OF 1	

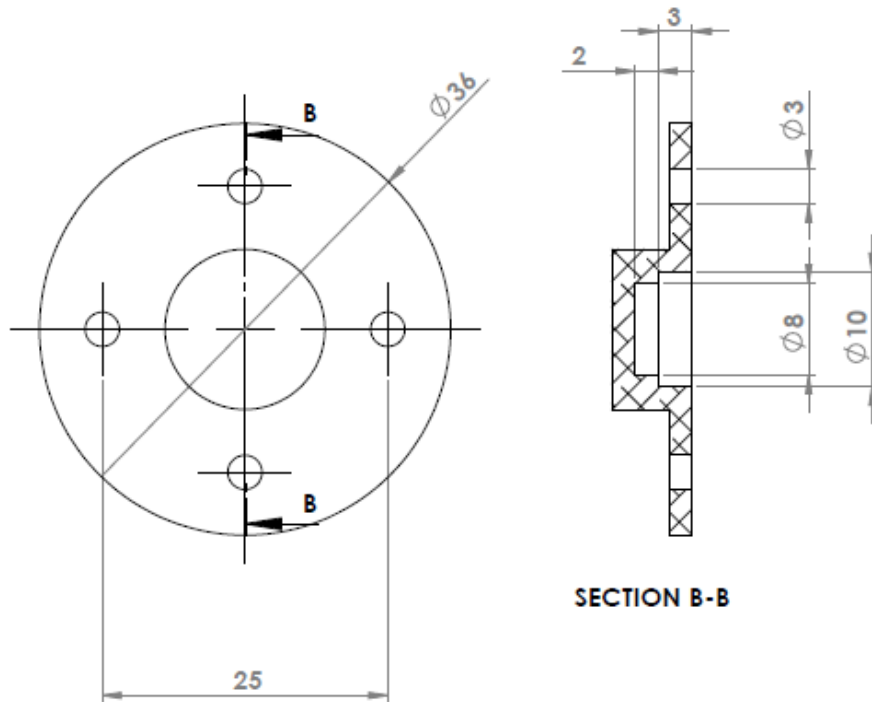
Housing brace



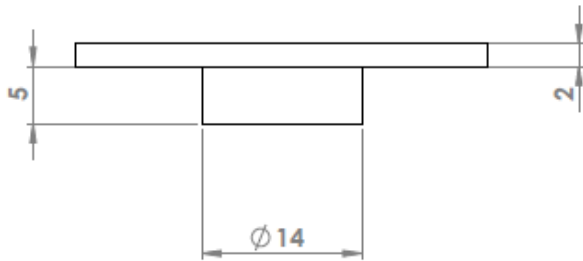
UNLESS OTHERWISE SPECIFIED: DIMENSIONS ARE IN MILLIMETERS		FINISH:		DEBUR AND BREAK SHARP EDGES		DO NOT SCALE DRAWING		REVISION	
SURFACE FINISH:									
TOLERANCES:									
LINEAR:									
ANGULAR:									
NAME		SIGNATURE		DATE		TITLE:			
DRAWN									
CHKD									
APPVD									
MFG									
Q.A						MATERIAL:		DWG. NO. Motor Stand-Off A4	
						WEIGHT:		SCALE: 1	
								SHEET 1 OF 1	



UNLESS OTHERWISE SPECIFIED: DIMENSIONS ARE IN MILLIMETERS		FINISH:		DEBUR AND BREAK SHARP EDGES		DO NOT SCALE DRAWING		REVISION	
SURFACE FINISH:									
TOLERANCES:									
LINEAR:									
ANGULAR:									
	NAME	SIGNATURE	DATE			TITLE:			
DRAWN									
CHK'D									
APP'VD									
MFG									
Q.A				MATERIAL:		DWG NO.		A4	
						Rotor Shaft			
				WEIGHT:		SCALE:2:1		SHEET 1 OF 1	



SECTION B-B



UNLESS OTHERWISE SPECIFIED: DIMENSIONS ARE IN MILLIMETERS SURFACE FINISH: TOLERANCES: LINEAR: ANGULAR:		FINISH:		DEBUR AND BREAK SHARP EDGES		DO NOT SCALE DRAWING		REVISION	
DRAWN		SIGNATURE		DATE		TITLE:			
CHK'D									
APP'VD									
MFG									
G.A.				MATERIAL:		DWG NO.		A4	
						SW3484			
				WEIGHT:		SCALE: 2:1		SHEET 1 OF 1	

APPENDIX D. VELOCITY DATA FOR 8,000 RPM OUTLET

	Span (5 mm Spacing)									
Width (4 mm Spacing)	0.00	0.00	1.21	12.67	17.77	9.15	9.81	26.48	25.03	33.54
	0.00	6.55	16.38	21.36	28.48	40.21	43.66	47.31	51.21	55.49
	0.00	0.00	0.00	0.00	15.73	32.28	38.54	46.78	51.37	53.60
	0.00	0.00	0.00	0.00	7.39	29.49	37.07	50.50	53.64	54.12
	0.00	0.00	0.00	0.00	0.00	22.90	31.69	45.97	47.57	48.60
	0.00	0.00	0.00	0.00	0.00	17.54	26.31	41.03	42.76	44.87
	0.00	0.00	0.00	0.00	0.00	11.61	21.29	35.88	38.67	41.47
	0.00	0.00	0.00	0.00	0.00	5.86	18.44	31.82	35.71	38.56
	0.00	0.00	0.00	0.00	0.00	0.00	15.05	28.19	32.27	34.96
	0.00	0.00	0.00	0.00	0.00	3.90	12.75	25.58	28.71	30.94
	0.00	0.00	0.00	0.00	0.00	0.00	11.41	22.43	25.72	27.81
	0.00	0.00	0.00	0.00	0.00	0.00	10.27	18.86	22.35	24.62
	0.00	0.00	0.00	0.00	0.00	2.89	9.56	16.91	19.52	22.06
	0.00	0.00	0.00	0.00	0.00	0.00	5.70	10.98	13.11	15.83
	0.00	0.00	0.00	0.00	0.00	0.00	0.00	0.00	0.00	0.00
	0.00	0.00	0.00	0.00	0.00	0.00	0.00	0.00	0.00	0.00

Span (5 mm Spacing)											
26.96	19.64	17.96	20.60	25.55	28.66	28.79	16.62	0.00	0.00	0.00	0.00
54.78	51.69	50.31	49.13	47.79	45.16	44.42	43.77	43.84	42.03	40.03	38.36
53.23	51.94	51.65	50.57	48.60	46.31	45.29	44.88	44.25	42.64	40.40	39.51
54.94	55.38	56.06	55.07	52.75	50.75	49.82	48.91	47.66	45.90	43.31	43.12
50.14	51.26	52.43	52.45	51.07	50.17	49.37	48.54	47.24	45.38	43.30	43.35
46.68	47.69	48.56	49.33	48.61	48.80	48.59	48.02	46.61	44.80	43.14	43.06
43.06	43.22	43.91	45.04	45.00	46.10	46.68	46.64	45.52	43.56	42.76	42.10
39.60	39.24	39.80	40.63	41.67	43.00	44.92	45.31	44.32	42.66	42.37	41.95
35.80	35.13	35.90	36.51	38.00	40.28	43.09	43.46	42.44	41.00	40.80	40.07
31.91	31.01	32.22	32.76	34.50	37.79	41.72	42.27	41.41	39.62	39.68	38.48
28.90	28.28	29.49	30.15	32.29	35.87	39.79	40.41	39.63	37.95	37.86	36.38
25.94	25.89	27.26	28.20	30.35	33.93	37.51	37.88	37.67	36.12	35.52	34.29
23.86	24.33	25.92	27.26	29.45	32.26	35.09	35.40	35.10	33.72	33.23	32.71
19.08	20.66	22.06	23.98	24.70	26.53	29.13	30.85	30.98	29.55	29.47	30.11
5.91	9.63	10.70	11.50	11.23	11.56	12.74	16.52	20.35	18.46	19.79	23.62
0.00	0.00	0.00	1.71	2.27	1.47	1.19	1.42	4.34	4.72	6.15	11.92

Span (5 mm Spacing)											
13.70	0.00	10.47	0.00	0.00	0.00	0.00	0.00	0.00	0.00	0.00	0.00
38.18	39.69	37.67	38.38	40.46	42.79	45.91	47.32	50.61	53.55	59.20	59.14
39.58	40.95	39.47	40.04	42.38	44.50	47.93	50.10	52.09	53.03	55.34	56.28
42.68	43.88	42.83	43.87	46.45	48.96	51.92	53.58	54.00	53.58	52.85	54.92
42.41	43.70	43.29	44.17	46.61	47.92	49.23	49.70	48.78	47.85	45.79	48.02
42.24	43.65	43.80	45.15	46.48	46.82	46.71	45.88	43.99	43.18	41.65	43.60
41.74	42.58	44.43	45.97	46.14	44.87	43.58	41.38	38.93	38.65	38.32	40.35
41.10	41.74	45.36	47.14	45.64	42.78	40.75	37.48	35.05	35.01	35.63	38.21
39.20	39.96	44.57	46.29	44.07	39.79	37.19	33.59	31.15	30.83	31.82	34.80
37.44	38.61	44.57	46.07	43.42	37.61	34.45	30.76	28.47	28.08	28.66	31.77
35.38	36.97	43.11	44.52	41.84	35.22	32.15	28.63	26.76	26.25	25.99	28.52
33.18	35.34	40.14	42.05	39.93	33.52	30.63	27.54	25.35	24.73	24.15	25.57
30.99	33.25	36.60	38.35	36.64	31.76	28.49	25.39	23.61	22.94	22.34	23.16
26.89	29.39	31.34	31.32	29.79	25.49	22.15	19.11	18.65	18.20	17.56	18.95
16.13	18.34	17.38	17.11	15.20	12.64	9.88	8.39	8.14	7.81	6.54	7.94
4.29	4.49	1.81	2.48	2.25	1.91	2.52	2.75	2.85	2.18	1.20	0.00

Span (5 mm Spacing)								
0.00	0.00	0.00	0.00	0.00	0.00	0.00	0.00	0.00
54.91	49.75	47.33	43.15	39.40	38.39	28.22	18.51	1.67
54.27	47.61	41.82	30.42	23.20	20.42	0.00	0.00	0.00
54.76	45.17	34.86	19.05	7.50	0.00	0.00	0.00	0.00
48.92	39.35	26.39	8.04	0.00	0.00	0.00	0.00	0.00
43.20	32.88	20.04	0.00	0.00	0.00	0.00	0.00	0.00
38.38	26.95	14.76	0.00	0.00	0.00	0.00	0.00	0.00
36.07	22.82	10.21	0.00	0.00	0.00	0.00	0.00	0.00
32.96	19.57	4.67	0.00	0.00	0.00	0.00	0.00	0.00
31.04	18.11	4.45	0.00	0.00	0.00	0.00	0.00	0.00
27.58	16.30	0.00	0.00	0.00	0.00	0.00	0.00	0.00
23.99	14.34	4.33	0.00	0.00	0.00	0.00	0.00	0.00
20.61	13.16	6.84	0.00	0.00	0.00	0.00	0.00	0.00
16.23	10.62	6.79	0.00	0.00	0.00	0.00	0.00	0.00
3.93	0.00	0.00	0.00	0.00	0.00	0.00	0.00	0.00
0.00	0.00	0.00	0.00	0.00	0.00	0.00	0.00	0.00

LIST OF REFERENCES

- [1] Naval Air System Command contract N00019-74-C-0434, *Multi-Bypass Ratio Propulsion System Technology Development*, Vol. I-III, Vought Systems Division, LTV Aerospace Corporation, 24 July 1975.
- [2] D.H. Gossett, "Investigation of cross flow fan propulsion for a lightweight VTOL aircraft," M.S. thesis, Department of Aeronautics and Astronautics, Naval Postgraduate School, Monterey, California, March 2000.
- [3] W. T. Cheng, "Experimental and numerical analysis of a crossflow fan," M.S. thesis, Department of Aeronautics and Astronautics, Naval Postgraduate School, Monterey, California, December 2003.
- [4] C. W. Schreiber, "Effect of span variation on the performance of a cross flow fan," M.S. thesis, Department of Mechanical and Astronautical Engineering, Naval Postgraduate School, Monterey, California, June 2006.
- [5] J. M. Ulvin, "Experimental investigation of a six inch diameter, four inch span cross-flow fan," M.S. thesis, Department of Mechanical and Astronautical Engineering, Naval Postgraduate School, Monterey, California, June 2008.
- [6] Antoniadis, "Numerical and experimental investigation of performance improvements of a cross-flow fan," M.S. thesis, Department of Mechanical and Aerospace Engineering, Naval Postgraduate School, Monterey, California, June 2010.
- [7] J. Kummer, "Propulsive wing," www.propulsivewing.com (last accessed May 15, 2012).
- [8] H. T. Yu, "Experimental investigation and numerical prediction of a cross-flow fan," M.S. thesis, Department of Mechanical and Astronautical Engineering, Naval Postgraduate School, Monterey, California, December 2006.

THIS PAGE INTENTIONALLY LEFT BLANK

INITIAL DISTRIBUTION LIST

1. Defense Technical Information Center
Ft. Belvoir, Virginia
2. Dudley Knox Library
Naval Postgraduate School
Monterey, California
3. Garth V. Hobson
Department of Mechanical and Aerospace Engineering
Naval Postgraduate School
Monterey, California
4. Anthony Gannon
Department of Mechanical and Aerospace Engineering
Naval Postgraduate School
Monterey, California
5. Mr. Leo Tin Boon
Temasek Defence Systems Institute
National University of Singapore
Singapore